**ECOLE POLYTECHNIQUE**

**CENTRE DE MATHÉMATIQUES APPLIQUÉES**
*UMR CNRS 7641*

91128 PALAISEAU CEDEX (FRANCE). Tél: 01 69 33 41 50. Fax: 01 69 33 30 11

http://www.cmap.polytechnique.fr/

# A stabilized discontinuous mortar formulation for elastostatics and elastodynamics problems Part II: discontinuous Lagrange multipliers

Patrice Hauret and Patrick Le Tallec

**R.I. N$^0$ 554** *September 2004*

# A stabilized discontinuous mortar formulation for elastostatics and elastodynamics problems Part II: discontinuous Lagrange multipliers

Patrice Hauret* Patrick Le Tallec†

September 27, 2004

**Abstract**

In this paper, we introduce, analyze and test first and second order stabilized discontinuous two-field mortar formulations for linearized elasticity problems, following the stabilization technique of Brezzi and Marini [BM00] introduced in the scalar elliptic case for a three-field formulation. All the fundamental assumptions arising in mortar formulations are proved for our discretization procedure. We also detail practical issues and present numerical tests to illustrate the analysis.

## 1 Introduction

In this paper, we introduce, analyze and test a non-conforming formulation using stabilized discontinuous mortar elements to find the vector solution $u$ of linearized elasticity problems such as:

$$\begin{cases} -\,div(\mathbf{E} : \varepsilon(u)) = f, \quad \Omega \subset \mathbb{R}^d, (d = 2, 3) \\ u = 0, \quad \Gamma_D, \\ (\mathbf{E} : \varepsilon(u)) \cdot n = g, \quad \Gamma_N, \end{cases} \tag{1}$$

where the linearized strain tensor is classically given by:

$$\varepsilon(u) = \frac{1}{2}\left(\nabla u + \nabla^t u\right),$$

and the fourth order elasticity tensor $\mathbf{E}$ is assumed to be elliptic over the set of symmetric matrices:

$$\exists \alpha > 0, \forall \xi \in \mathbb{R}^{d\times d}, \xi^t = \xi, \quad (\mathbf{E} : \xi) : \xi \geq \alpha\, \xi : \xi.$$

*CMAP, Ecole Polytechnique, 91 128 Palaiseau, France. patrice.hauret@polytechnique.fr
†LMS, Ecole Polytechnique, 91 128 Palaiseau, France. patrick.letallec@polytechnique.fr

The analysis is also extended to the elastodynamics problem:

$$\begin{cases} \rho \dfrac{\partial^2 u}{\partial t^2} - div(\mathbf{E} : \varepsilon(u)) = f, \quad [0,T] \times \Omega, \\ u = 0, \quad [0,T] \times \Gamma_D, \\ (\mathbf{E} : \varepsilon(u)) \cdot n = g, \quad [0,T] \times \Gamma_N, \\ u = u_0, \quad \{0\} \times \Omega, \\ \dfrac{\partial u}{\partial t} = \dot{u}_0, \quad \{0\} \times \Omega, \end{cases} \tag{2}$$

and we consider this analysis as a theoretical background for using discontinuous mortar elements in nonlinear elastodynamics.

Mortar methods have been introduced for the first time in [BMP93, BMP94] as a weak coupling between subdomains with nonconforming meshes, or between subproblems solved with different approximation methods. The main purpose was to overcome the very sub-optimal "$\sqrt{h}$" error estimate obtained with pointwise matching. The analysis of this method as a mixed formulation was first made in [Bel99].

Nevertheless, in spite of the optimal error convergence obtained with the original mortar elements, some numerical difficulties appear. First, the original space of Lagrange multipliers ensuring the weak coupling is rather difficult to build in 3D on the boundary of the interfaces when more than two subdomains have a common intersection (see [BM97, BD98]). Moreover, the original constrained space has a non-local basis on the non-conforming artificial interfaces, which may lead to small spurious oscillations of the approximate solution.

To overcome the first difficulty, one idea is given in [Ses98] when displacements are at least approximated by second order polynomials. The introduced Lagrange multipliers have a lower order, still enabling optimal error estimates, and no special treatment is needed on the boundary of the interfaces. To overcome the second difficulty, dual mortar spaces are proposed in [Woh00, Woh01], enabling the localization of the mortar kinematical constraint. In order to benefit from the advantages of these two approaches, we propose to introduce stabilized low order discontinuous mortar elements. This idea has already been introduced for a first order three-field mortar formulation in [BM00], and we exploit it herein in the two-field framework for first and second order elements when dealing with elastostatics and elastodynamics problems.

In a previous paper (Part I: abstract framework), we have proved that under general assumptions, not only the mortar formulation is well-posed and achieves optimal accuracy in the elastostatics framework (cf. [Woh01]), but such a result also holds in the elastodynamics framework. Moreover, the quality of the approximation was proved not to be affected by the number and the size of the subdomains.

In section 2, the fundamental assumptions and results arising in mortar element methods to approximate the solution of the elastostatics (1) and elastodynamics (2) problems are recalled. We propose in section 3 the analysis of stabilized discontinuous mortar elements, proving the satisfaction of the fundamental assumptions. In section 4, some practical issues are pointed out: the choice of an appropriate penalization term, and the exact integration of the constraint. We present numerical tests in section 5 to confirm the previous analysis.

# 2 Nonconforming setting

## 2.1 Position of the problem

Let $\Omega \subset \mathbb{R}^d$ $(d = 2, 3)$, be an open set partitioned into $K$ subsets $(\Omega_k)_{1\leq k\leq K}$. We denote by $\gamma_{kl} = \overline{\Omega_k} \cap \overline{\Omega_l}$ the interface between $\Omega_k$ and $\Omega_l$, and the skeleton of the internal interfaces is denoted by $\mathcal{S} = \bigcup_{k,l\geq 1} \gamma_{kl}$. Concerning the coefficients of the fourth order elasticity tensor $\mathbf{E}$, we assume that the stress tensor is symmetric whatever the deformation is in the material, namely for almost all $x \in \Omega$:

$$\forall \xi \in \mathbb{R}^{d\times d}, \xi^t = \xi, \quad \mathbf{E}(x) : \xi \text{ is a symmetric matrix.}$$

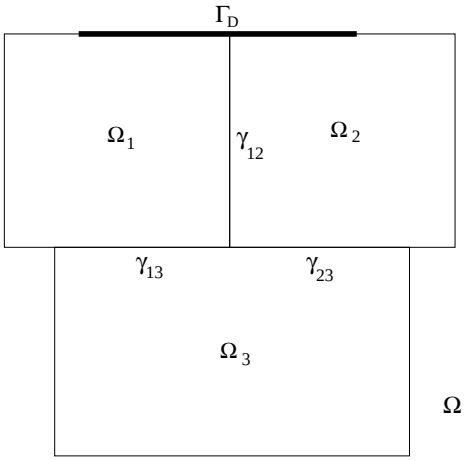


Figure 1: A decomposition of $\Omega$ into subdomains.

We introduce the following spaces:

$$H^1_*(\Omega) = \{v \in H^1(\Omega)^d,\ v|_{\Gamma_D} = 0\},$$

$$H^1_*(\Omega_k) = \{v \in H^1(\Omega_k)^d,\ v|_{\Gamma_D\cap\partial\Omega_k} = 0\},$$

$$X = \left\{v \in L^2(\Omega)^d, \quad v_k = v|_{\Omega_k} \in H^1_*(\Omega_k), \forall k\right\} = \prod_{k=0}^{K} H^1_*(\Omega_k),$$

$X$ being endowed with the $H^1$ broken norm:

$$\|v\|_X = \left(\sum_{k=0}^{K} \|v\|^2_{H^1(\Omega_k)^d}\right)^{\frac{1}{2}}.$$

Here, in order to be scale independent when dealing with a large number of subdomains, we use a scale invariant definition of the $H^1$ norm:

$$\|v\|^2_{H^1(\Omega_k)^d} = \frac{1}{(L_k)^2}\|v\|^2_{L^2(\Omega_k)^d} + \|\nabla v\|^2_{L^2(\Omega_k)^{d\times d}},$$

$L_k$ being a characteristic length of $\Omega_k$, for instance its diameter.
Within a given translation handling non-homogeneous boundary conditions, the elastostatic problem looks for $u \in H^1_*(\Omega)$ such that:

$$a(u,v) = l(v), \quad \forall v \in H^1_*(\Omega), \tag{3}$$

where the continuous coercive bilinear form $a$ is defined by:

$$a(u,v) = \int_\Omega (\mathbf{E} : \varepsilon(u)) : \varepsilon(v), \quad \forall u, v \in H^1_*(\Omega),$$

and the continuous linear form $l$ by:

$$l(v) = \int_\Omega f \cdot v + \int_{\Gamma_N} g \cdot v, \quad \forall v \in H^1_*(\Omega).$$

This problem is classically well-posed by Lax-Milgram lemma, the Korn's inequality (see [DL72]) ensuring the coercivity of the bilinear form $a$ over $H^1_*(\Omega) \times H^1_*(\Omega)$. Similarly, the problem in elastodynamics looks for:

$$u \in \mathcal{C}^0(0,T; H^1_*(\Omega)) \cap \mathcal{C}^1(0,T; L^2(\Omega)^d),$$

such that in the sense of distributions on $]0,T[$:

$$\frac{\partial^2}{\partial t^2} \int_\Omega \rho u(t) \cdot v + a(u(t), v) = \int_\Omega f(t) \cdot v + \int_{\Gamma_N} g(t) \cdot v, \qquad \forall v \in H^1_*(\Omega). \tag{4}$$

## 2.2 Discretization

We introduce here a non-conforming discretization of the problem (3) using mortar elements to be further defined later on.

### 2.2.1 The mesh

As in Part I, for each $1 \leq k \leq K$, we consider a family of shape regular *affine meshes* $(\mathcal{T}_{k;h_k})_{h_k>0}$ on the subdomain $\Omega_k$. This means that each element $T$ is the image of a reference element $\hat{T}$ by an affine mapping $J_T$. For each $T \in \mathcal{T}_{k;h_k}$, we will denote its diameter:

$$h(T) = diam(T),$$

and the local mesh size by:

$$h_k = \sup_{T \in \mathcal{T}_{k;h_k}} h(T).$$

Then, a nonconforming family of meshes $(\mathcal{T}_h)_{h>0}$ over $\Omega$ is obtained by:

$$\mathcal{T}_h = \bigcup_{k=1}^{K} \mathcal{T}_{k,h_k}, \quad h = \max_{1 \leq k \leq K} h_k.$$

The skeleton $\mathcal{S} = \bigcup_{k,l \geq 1} \gamma_{kl}$ is partitioned into $M$ interfaces $(\Gamma_m)_{1 \leq m \leq M}$, and can then be decomposed as $\mathcal{S} = \bigcup_{1 \leq m \leq M} \Gamma_m$. Moreover, we assume that for each $1 \leq m \leq M$,

there exists at least one domain $\Omega_k$ with $k \geq 1$ such that $\Gamma_m \subset \partial\Omega_k$, and denote $k(m) := k$ the name of one of these subdomains, taken once for all for each interface. This side will said to be the non-mortar (or slave) side.

For each $1 \leq m \leq M$, $\Gamma_m$ inherits a family of meshes $(\mathcal{F}_{m;\delta_m})_{\delta_m>0}$, obtained as the trace of the volumic mesh $(\mathcal{T}_{k(m);h_{k(m)}})_{h_{k(m)}>0}$ of the slave subdomain over $\Gamma_m$. We have denoted by:

$$\delta_m = \sup_{F\in\mathcal{F}_{m;\delta_m}} h(F).$$

We also denote by $\overline{\delta}_m$ the size of the mesh on the mortar side:

$$\overline{\delta}_m = \sup_{T\in\mathcal{T}_{l;h_l}, l\neq k(m)} diam(T\cap\Gamma_m).$$

Then, a family of interface meshes $(\mathcal{F}_\delta)_{\delta>0}$ can be defined over $\mathcal{S}$ by:

$$\mathcal{F}_\delta = \bigcup_{m=1}^{M} \mathcal{F}_{m;\delta_m}, \quad \delta = \max_{1\leq m\leq M} \delta_m.$$

For each $F \in \mathcal{F}_{m;\delta_m}$, we denote by $T(F) \in \mathcal{T}_{k(m);h_{k(m)}}$ the unique element $T \in \mathcal{T}_{k(m);h_{k(m)}}$ such that $T \cap \mathcal{S} = F$.
Moreover, we recall that we have assumed in Part I that:

**Assumption 1.** *$F \in \mathcal{F}_\delta$ is always an entire face of $T(F) \in \mathcal{T}_h$.*

In other words, the construction of the interfaces $(\Gamma_m)_{1\leq m\leq M}$ respects the mesh of the slave sides.

**Remark 1.** *For simplicity, the mesh is assumed to be affine but the following results are still valid for regular quasi-uniform quadrangular meshes, at least in 2D (see [GR86]). In fact, the only assumptions to satisfy are the following standard inequalities:*

$$\begin{cases} |\hat{w}|_{H^m(\hat{K})} \leq C\ diam(K)^m meas(K)^{-\frac{1}{2}} |w|_{H^m(K)}, \\ |w|_{H^m(K)} \leq C\ diam(K)^{-m} meas(K)^{\frac{1}{2}} |\hat{w}|_{H^m(\hat{K})}, \end{cases}$$

*between the semi-norms of the function $w$ defined on a mesh-element $K$ and its transformation $\hat{w}$ defined on the corresponding reference element $\hat{K}$.*

**Remark 2.** *In the following sections, $C$ will stand for various constants independent of the discretization.*

### 2.2.2 Interface mesh-dependent spaces

As in Part I, we also use mesh-dependent trace spaces, endowed with useful mesh-dependent norms already introduced and used in [AT95, Woh99]. For each $1 \leq m \leq M$, they are defined by:

$$\mathbb{H}^{1/2}_\delta(\Gamma_m) = \{\phi \in L^2(\Gamma_m)^d, \|\phi\|^2_{\delta,\frac{1}{2},m} = \sum_{F\in\mathcal{F}_{m;\delta_m}} \frac{1}{h(F)} \|\phi\|^2_{L^2(F)^d} < +\infty\},$$

$$\mathbb{H}_\delta^{-1/2}(\Gamma_m) = \{\lambda \in L^2(\Gamma_m)^d, \|\lambda\|^2_{\delta,-\frac{1}{2},m} = \sum_{F\in\mathcal{F}_{m;\delta_m}} h(F)\|\lambda\|^2_{L^2(F)^d} < +\infty\},$$

endowed respectively with the norms $\|\cdot\|_{\delta,\frac{1}{2},m}$ and $\|\cdot\|_{\delta,-\frac{1}{2},m}$. The product spaces $\mathbb{W}_\delta = \prod_{k=1}^K \mathbb{H}_\delta^{1/2}(\Gamma_m)$ and $\mathbb{M}_\delta = \prod_{k=1}^K \mathbb{H}_\delta^{-1/2}(\Gamma_m)$, are then respectively endowed with the norms:

$$\|\phi\|_{\delta,\frac{1}{2}} = \left(\sum_{m=1}^M \|\phi\|^2_{\delta,\frac{1}{2},m}\right)^{1/2},$$

$$\|\lambda\|_{\delta,-\frac{1}{2}} = \left(\sum_{m=1}^M \|\lambda\|^2_{\delta,-\frac{1}{2},m}\right)^{1/2}.$$

## 2.3 Approximate problem

### 2.3.1 Nonconforming formulation

Let us define the discrete subspaces of degree $q$ inside each subdomain :

$$X_{k;h_k} = \{p \in H^1_*(\Omega_k)\cap \mathcal{C}^0(\Omega_k)^d, \quad p|_T \in \mathcal{P}_q(T), \forall T \in \mathcal{T}_{k;h_k}\} \oplus \mathcal{B}_{k;h_k},$$

with $\mathcal{P}_q = [\mathbb{P}_q]^d$ or $[\mathbb{Q}_q]^d$. We have denoted by $\mathbb{P}_q$ (resp. $\mathbb{Q}_q$) the space of polynomials of total (resp. partial) degree $q$. The local space $\mathcal{B}_{k;h_k}$ of interface bubble stabilization will be constructed later on. The corresponding product space is denoted by:

$$X_h = \prod_{k=0}^K X_{k;h_k} \subset X.$$

We introduce the following trace spaces on the non-mortar side:

$$W_{m;\delta_m} = \{p|_{\Gamma_m}, p \in X_{k(m);h_{k(m)}}\}, \qquad W^0_{m;\delta_m} = W_{m;\delta_m} \cap H^1_0(\Gamma_m)^d,$$

and the corresponding product space $W^0_\delta = \prod_{m=1}^M W^0_{m;\delta_m}$ endowed with the mesh-dependent norm $\|\cdot\|_{\delta,\frac{1}{2}}$.

In order to formulate the weak continuity constraint, the following spaces of discontinuous Lagrange multipliers are defined:

$$M_{m;\delta_m} = \{p \in L^2(\Gamma_m)^d, \quad p|_F \in \mathcal{P}_{q-1}(F), \forall F \in \mathcal{F}_{m,\delta_m}\}, \tag{5}$$

as well as the product space $M_\delta = \prod_{m=1}^M M_{m;\delta_m}$, endowed with the mesh-dependent norm $\|\cdot\|_{\delta,-\frac{1}{2}}$ and $M = \prod_{m=1}^M L^2(\Gamma_m)^d$. The following continuous bilinear form is then classically introduced:

$$\begin{aligned} b: \quad X \times M \quad &\to \mathbb{R} \\ (v,\lambda) \quad &\mapsto b(v,\lambda) = \sum_{m=1}^M \int_{\Gamma_m} [v]_m \cdot \lambda_m, \end{aligned}$$

with $[v]_m = v_{k(m)} - v_l$ denoting the jump on $\gamma_{k(m)l} \subset \Gamma_m$. Then, the constrained space of discrete unknowns can be defined as in Part I by:

$$V_h = \{u_h \in X_h, b(u_h, \lambda_h) = 0, \quad \forall \lambda_h \in M_\delta\}.$$

In order to formulate the non-conforming approximate problem, it is standard to consider the broken elliptic form:

$$\begin{aligned} \tilde{a}: \quad X \times X \quad &\to \mathbb{R} \\ (u, v) \quad &\mapsto \tilde{a}(u, v) = \sum_{k=1}^{K} a_k(u_k, v_k), \end{aligned}$$

with:

$$a_k(u_k, v_k) = \int_{\Omega_k} (\mathbf{E} : \varepsilon(u_k)) : \varepsilon(v_k).$$

We are then interested in finding $(u_h, \lambda_h) \in X_h \times M_\delta$, such that:

$$\begin{cases} \tilde{a}(u_h, v_h) + b(v_h, \lambda_h) = l(v_h), \quad \forall v_h \in X_h, \\ b(u_h, \mu_h) = 0, \quad \forall \mu_h \in M_\delta. \end{cases} \tag{6}$$

In other words, we solve our variational problem on the product space $X_h$ under the kinematic continuity constraint $b(\cdot, \cdot) = 0$, with a corresponding formulation for the elastodynamics case (see Part I, equation 34).

### 2.3.2 Fundamental assumptions

The analysis of Part I was relying on the following fundamental assumption, concerning the compatibility of $X_h$ and $M_\delta$:

**Assumption 2.** *For each interface $1 \leq m \leq M$, there exists an operator:*

$$\pi_m : \mathbb{H}_\delta^{1/2}(\Gamma_m) \to W_{m;\delta_m}^0,$$

*such that for all $v \in \mathbb{H}_\delta^{1/2}(\Gamma_m)$:*

$$\int_{\Gamma_m} (\pi_m v) \cdot \mu = \int_{\Gamma_m} v \cdot \mu, \quad \forall \mu \in M_{m;\delta_m},$$

*with:*

$$\|\pi_m v_m\|_{\delta,\frac{1}{2},m} \leq C_m \|v\|_{\delta,\frac{1}{2},m}.$$

This assumption means that the projection perpendicular to the multiplier space onto the trace space $W_{m;\delta_m}^0$ with zero extension is continuous. This assumption must be checked for each choice of discretization. Its major consequence lies in the fact that the weak-continuity constraint is onto, as shown in Part I.
Under assumptions 1 and 2 and additional hypothesis mainly dealing with the geometry of the partition, it can be shown (Part I) that:

- the discrete problem (6) is well-posed,
- the solution $(u_h, \lambda_h) \in X_h \times M_\delta$ of (6) is an optimal approximation of the displacements $u \in H^1_*(\Omega)$ solution of (6), and of their fluxes ($\lambda = \nabla u \cdot n$) through the artificial interfaces,
- the discrete solution in displacements $u_n^h \in V_h$ and velocities $\dot{u}_n^h \in V_h$, $0 \leq n \leq T/\Delta t$ of:

$$\begin{cases} \displaystyle\int_\Omega \rho \frac{\dot{u}_{n+1}^h - \dot{u}_n^h}{\Delta t} \cdot v_h + \tilde{a}\left(\frac{u_n^h + u_{n+1}^h}{2}, v_h\right) = \frac{L_n(v_h) + L_{n+1}(v_h)}{2}, \qquad \forall v_h \in V_h, \\ \displaystyle\frac{u_{n+1}^h - u_n^h}{\Delta t} = \frac{\dot{u}_n^h + \dot{u}_{n+1}^h}{2}, \end{cases} \tag{7}$$

  is an optimal approximation in space and time of the solution of (2), where we have introduced the virtual work of the applied forces at the discrete time $t_n = n\Delta t$:

$$L_n(v_h) = \int_\Omega f(t_n) \cdot v_h + \int_{\Gamma_N} g(t_n) \cdot v_h, \quad \forall v_h \in V_h,$$

- such properties are not affected by the number $K$ and the size of the subdomains.

# 3 Analysis of discontinuous mortar spaces

In this section, the fundamental assumption 2 on mortar spaces is checked for particular discrete spaces with discontinuous Lagrange multipliers, when a suitable stabilization on the interface is added. Let us mention (see Part I) that this assumption is equivalent to the following interface inf-sup conditions for $1 \leq m \leq M$:

$$\inf_{\mu_m \in M_{m;\delta_m}} \sup_{\phi_m \in W^0_{m;\delta_m}} \frac{\displaystyle\int_{\Gamma_m} \mu_m \cdot \phi_m}{\|\mu_m\|_{\delta,-\frac{1}{2},m} \|\phi_m\|_{\delta,\frac{1}{2},m}} \geq \beta'_m. \tag{8}$$

In subsection 3.1, we show that a $\mathbb{P}_1/\mathbb{P}_0$ approximation with interface bubble stabilization on $u_h$ is compatible for $u/\lambda$, i.e satisfies assumption 2. This idea has been introduced in [BM00] for the so-called three-field formulation. In subsection 3.3, we propose a numerical procedure to check the compatibility condition (8). In subsection 3.4, we show a useful lemma enabling to check only a local inf-sup condition on the interface in the way of [BN83, Ste84, Ste90] for divergence free problems. We use it in the subsection 3.5 to prove (8) for a stabilized $\mathbb{P}_2$ or $\mathbb{Q}_2/\mathbb{P}_1 -$ *discontinuous* formulation.

## 3.1 Stabilized first order elements

Here, we assume that $\lambda$ is approximated by piecewise constants ($q = 1$), and $u$ by continuous piecewise linear functions with bubbles on the interface $\mathcal{S}$ (see figure 2). For each mesh element $F \in \mathcal{F}_\delta$ on the interface $\mathcal{S}$, an interface bubble can be defined

on $T(F)$ in the way followed by [BM00]. If $T(F)$ is a triangle or a tetrahedron whose vertices are denoted by $(a_i)_i$ with the associated barycentric coordinates $(\lambda_i)_i$, an interface bubble $b_F$ can be defined as:

$$b_F = \prod_{a_i \in \mathcal{S}} \lambda_i.$$

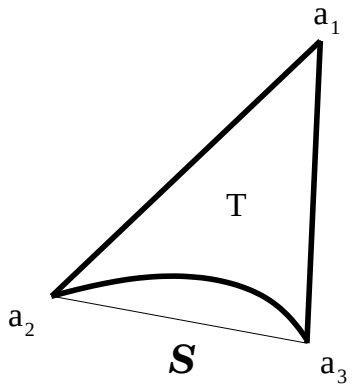


Figure 2: Bubble function $\lambda_2\lambda_3$ on the interface $\mathcal{S}$, in a triangle $T$. (Bidimensional problems)

When considering a square or cubic reference element $\hat{Q} = [-1,1]^d$, we can also define the face bubble associated with the face $\hat{F} = [-1,1]^{d-1} \times \{-1\}$

- for $d = 3$ by:

$$b_{\hat{F}} = \frac{1}{2}(1-x_1^2)(1-x_2^2)(1-x_3), \qquad \forall \hat{x} = (\hat{x}_1, \hat{x}_2, \hat{x}_3) \in [-1,1]^3,$$

- for $d = 2$ by:

$$b_{\hat{F}} = \frac{1}{2}(1-x_1^2)(1-x_2), \qquad \forall \hat{x} = (\hat{x}_1, \hat{x}_2) \in [-1,1]^2.$$

**Proposition 1.** *With $q = 1$ and a bubble stabilization on the interface, the assumption 2 is always satisfied with a stability constant independent of the discretization, whatever the relative configuration of the meshes on the interface $\mathcal{S}$.*

**Proof :** Let $I_m$ be an approximation operator from $\mathbb{H}_\delta^{1/2}(\Gamma_m)$ to $W^0_{m;\delta_m}$, to be detailed later. For all $v \in \mathbb{H}_\delta^{1/2}(\Gamma_m)$, we define with constants $\gamma_F$ to be computed later:

$$\pi_m v = I_m v + \sum_{F \in \mathcal{F}_{m;\delta_m}} \gamma_F b_F\big|_F.$$

Because Lagrange multipliers are piecewise constant, we must have for all $F \in \mathcal{F}_{m;\delta_m}$:

$$\int_F \pi_m v = \int_F v,$$

which imposes:

$$\gamma_F = \frac{\int_F (v - I_m v)}{\int_F b_F}.$$

By a classical change of variable on the reference element $\hat{F}$:

$$\int_F b_F = \frac{meas(F)}{meas(\hat{F})} \int_{\hat{F}} \hat{b} = C\, meas(F),$$

and then by Cauchy-Schwartz inequality:

$$|\gamma_F| \leq C \frac{\|v - I_m v\|_{L^2(F)}}{meas(F)^{1/2}}.$$

Thus, we obtain the following estimate:

$$\begin{aligned}
\|\pi_k v\|^2_{\delta,\frac{1}{2},m} &= \sum_{F \in \mathcal{F}_{m;\delta_m}} \frac{1}{h(F)} \|\pi_k v\|^2_{L^2(F)} \\
&\leq C \left( \sum_{F \in \mathcal{F}_{m;\delta_m}} \frac{1}{h(F)} \|I_m v\|^2_{L^2(F)} + \sum_{F \in \mathcal{F}_{m;\delta_m}} \frac{1}{h(F)} \|v - I_m v\|^2_{L^2(F)} \frac{\|b_F\|^2_{L^2(F)}}{meas(F)} \right) \\
&\leq C \left( \sum_{F \in \mathcal{F}_{m;\delta_m}} \frac{1}{h(F)} \|I_m v\|^2_{L^2(F)} + \sum_{F \in \mathcal{F}_{m;\delta_m}} \frac{1}{h(F)} \|v - I_m v\|^2_{L^2(F)} \right) \\
&\leq C \left( \sum_{F \in \mathcal{F}_{m;\delta_m}} \frac{1}{h(F)} \|I_m v\|^2_{L^2(F)} + \sum_{F \in \mathcal{F}_{m;\delta_m}} \frac{1}{h(F)} \|v\|^2_{L^2(F)} \right).
\end{aligned}$$

By chosing the approximation operator $I_m$ as the projection from $\mathbb{H}^{1/2}_{\delta}(\Gamma_m)$ to $W^0_{m;\delta_m}$ for the inner product:

$$\langle u, v \rangle_{\delta,\frac{1}{2},m} = \sum_{F \in \mathcal{F}_{m;\delta_m}} \frac{1}{h(F)} \int_F u \cdot v,$$

which ensures that we have:

$$\sum_{F \in \mathcal{F}_{m;\delta_m}} \frac{1}{h(F)} \|I_m v\|^2_{L^2(F)} \leq \sum_{F \in \mathcal{F}_{m;\delta_m}} \frac{1}{h(F)} \|v\|^2_{L^2(F)},$$

we conclude:

$$\|\pi_m v\|_{\delta,\frac{1}{2},m} \leq C \|v\|_{\delta,\frac{1}{2},m},$$

which ends the proof. □

### 3.2 A counter example

We show here that the assumption 2 can be easily violated when a bubble stabilization is not introduced. For example, let us consider an interface $\mathcal{S}$ whose non-mortar side is represented on figure 3, and equipped with a uniform square mesh. The diameter of the squares is denoted by $\delta$.
We adopt the classical $\mathbb{Q}_1 \times \mathbb{P}_0$ discretization:

$$\begin{cases} M_\delta = \{p \in L^2(\mathcal{S})^d, \quad p|_F \in \mathbb{P}_0(F)^d, \forall F \in \mathcal{F}_\delta\}, \\ W_\delta^0 = \{p \in H_0^1(\mathcal{S})^d \cap \mathcal{C}^0(\mathcal{S})^d, \quad p|_F \in \mathbb{Q}_1(F)^d, \forall F \in \mathcal{F}_\delta\}. \end{cases}$$

If $\lambda_h^* \in M_\delta$ is taken as a checkaboard (as shown on figure 3), that is:

$$\lambda_h^*|_F = \pm a, \quad a \in \mathbb{R}^d,$$

depending of $F \in \mathcal{F}_\delta$ in the way indicated by figure 3, then we have by point symmetry of each shape function around each node:

$$\int_{\mathcal{S}} \phi_h \cdot \lambda_h^* = 0, \quad \forall \phi_h \in W_\delta^0.$$

As a consequence, the inf-sup condition (8) cannot be satisfied.

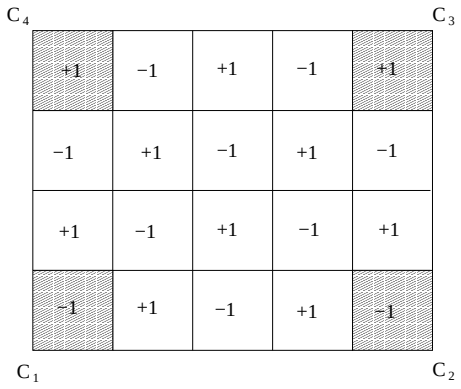


Figure 3: Uniform square mesh of the interface $\mathcal{S}$ between two subdomains.

**Remark 3.** *The standard assumption 2 ensures the well-posedness of the approximate problem (6) whatever the relative configuration of the mortar and non-mortar meshes. In particular, it is always strictly stronger than the strictly sufficient inf-sup condition:*

$$\inf_{\lambda_h \in M_\delta \setminus \{0\}} \sup_{u_h \in X_h \setminus \{0\}} \frac{b(u_h, \lambda_h)}{\|\lambda_h\|_{\delta,-\frac{1}{2}} \|u_h\|_X} \geq \beta, \tag{9}$$

*except in the conforming case, where it is equivalent. The instability shown on figure 3 entails that (6) is not well-posed for conforming meshes on the interface, but*

*the problem (6) could be well-posed for strictly non-conforming interfaces. Indeed, in the inf-sup condition (9), the displacement over the interface enters through its jump whereas it only enters in the assumption 2 through its value on the non-mortar side. Obviously, the space of jumps over the interface can be considerably richer than the space of the displacements on the non-mortar side if the interface is really non-conforming. This enrichment coming from the non-conformity can make the inf-sup condition (9) satisfied, but in such cases, there will be no robustness with respect to the relative position of the interfaces.*

### 3.3 Numerical validation

We propose here a numerical test to check if the inf-sup condition (8) is satisfied for a given discretization by mesh-refinement. This test is a simple variant of a test introduced by [BCI00]. For $1 \leq m \leq M$, let us denote by:

$$\beta'_{m;\delta_m} = \min_{\lambda_m \in M_{m;\delta_m} \setminus \{0\}} \max_{\phi_m \in W^0_{m;\delta_m} \setminus \{0\}} \frac{\displaystyle\int_{\Gamma_m} \lambda_m \cdot \phi_m}{\|\phi_m\|_{\delta,\frac{1}{2},m} \|\lambda_m\|_{\delta,-\frac{1}{2},m}},$$

the discrete inf-sup constant. Then, we have the following result:

**Proposition 2.** *Under the assumption that the family of meshes $(\mathcal{F}_{m;\delta_m})_{\delta_m>0}$ on the interface $\Gamma_m$ is quasi-uniform, we have:*

$$\beta'_{m;\delta_m} = O\left(\frac{1}{\delta_m^{d-1}} \lambda_{min}(\mathbf{B}_m \mathbf{B}_m^t)^{1/2}\right),$$

*where $\mathbf{B}_m$ is the matrix associated to the bilinear form $b$ on $W^0_{m;\delta_m} \times M_{m;\delta_m}$ and $\lambda_{min}(\mathbf{M})$ the smallest eigenvalue of the matrix $\mathbf{M}$. We remark that $\lambda_{min}(\mathbf{B}_m \mathbf{B}_m^t)^{1/2}$ is the smallest positive singular value of $\mathbf{B}_m$.*

**Proof :** We have $\beta'_{m;\delta_m} = \min_{\lambda_m \in M_{m;\delta_m} \setminus \{0\}} A_{\lambda_m}$ with:

$$A_{\lambda_m} = \max_{\phi_m \in W^0_{m;\delta_m} \setminus \{0\}} \frac{\displaystyle\int_{\Gamma_m} \lambda_m \cdot \phi_m}{\|\phi_m\|_{\delta,\frac{1}{2},m} \|\lambda_m\|_{\delta,-\frac{1}{2},m}}.$$

Using matrices and vectors representing data in the chosen discrete spaces in a given basis, we have:

$$A_{\lambda_m} = \max_{\Phi_m} \frac{\langle \mathbf{B}\Phi_m, \Lambda_m \rangle}{\langle \mathbf{M}_\Phi \Phi_m, \Phi_m \rangle^{1/2} \langle \mathbf{M}_\Lambda \Lambda_m, \Lambda_m \rangle^{1/2}}.$$

In particular, the matrix $\mathbf{M}_\Phi$ (resp. $\mathbf{M}_\Lambda$) is the definite positive matrix representing $\|\cdot\|_{\delta,\frac{1}{2},m}$ (resp. $\|\cdot\|_{\delta,-\frac{1}{2},m}$) in the discrete spaces. Let us remark that $\mathbf{B}$, $\mathbf{M}_\Phi$ and $\mathbf{M}_\Lambda$ depend on $h$. The vector $\Phi_m$ reaches the maximum if:

$$\langle \mathbf{B}\Psi_m, \Lambda_m \rangle - s \langle \mathbf{M}_\Phi \Phi_m, \Psi_m \rangle = 0, \quad \forall \Psi_m,$$

with $\langle \mathbf{M}_\Phi \Phi_m, \Phi_m \rangle = 1$. As a consequence:

$$\Phi_m = \frac{\mathbf{M}_\Phi^{-1} \mathbf{B}^t \Lambda_m}{\left\langle \mathbf{B}\mathbf{M}_\Phi^{-1}\mathbf{B}^t \Lambda_m, \Lambda_m \right\rangle^{1/2}},$$

and:

$$\begin{aligned} A_{\lambda_m} &= \frac{\left\langle \mathbf{B}\mathbf{M}_\Phi^{-1}\mathbf{B}^t \Lambda_m, \Lambda_m \right\rangle^{1/2}}{\langle \mathbf{M}_\Lambda \Lambda_m, \Lambda_m \rangle^{1/2}} \\ &\leq \frac{1}{\lambda_{min}(\mathbf{M}_\Phi)^{1/2}} \frac{1}{\lambda_{min}(\mathbf{M}_\Lambda)^{1/2}} \frac{\langle \mathbf{B}\mathbf{B}^t \Lambda_m, \Lambda_m \rangle^{1/2}}{\langle \Lambda_m, \Lambda_m \rangle^{1/2}}, \quad \forall \Lambda_m. \end{aligned}$$

The last result is a consequence of the inequality:

$$\lambda_{min}(\mathbf{M}) \langle \Lambda, \Lambda \rangle \leq \langle \mathbf{M}\Lambda, \Lambda \rangle \leq \lambda_{max}(\mathbf{M}) \langle \Lambda, \Lambda \rangle .$$

Hence we get:

$$\beta'_{m;\delta_m} = \min_{\lambda_m \in M_{m;\delta_m} \setminus \{0\}} A_{\lambda_m} \leq C \frac{1}{\delta_m^{d-1}} \lambda_{min}(\mathbf{B}_m \mathbf{B}_m^t)^{1/2},$$

using the result from lemma 1, because the interface mesh is quasi-uniform.

Conversely, proceeding as previously, we deduce that:

$$\begin{aligned} A_{\lambda_m} &= \frac{\left\langle \mathbf{B}\mathbf{M}_\Phi^{-1}\mathbf{B}^t \Lambda_m, \Lambda_m \right\rangle^{1/2}}{\langle \mathbf{M}_\Lambda \Lambda_m, \Lambda_m \rangle^{1/2}} \\ &\geq C \frac{1}{\lambda_{max}(\mathbf{M}_\Phi)^{1/2}} \frac{1}{\lambda_{max}(\mathbf{M}_\Lambda)^{1/2}} \frac{\langle \mathbf{B}\mathbf{B}^t \Lambda_m, \Lambda_m \rangle^{1/2}}{\langle \Lambda_m, \Lambda_m \rangle^{1/2}}, \end{aligned}$$

yielding:

$$\beta'_{m;\delta_m} \geq C \frac{1}{\delta_m^{d-1}} \lambda_{min}(\mathbf{B}_m \mathbf{B}_m^t)^{1/2},$$

using lemma 1 on a quasi-uniform mesh. Hence the proof. □

In the previous proof, we have used the following lemma:

**Lemma 1.** *We assume that $\mathcal{F}_{m;\delta_m}$ is a family of uniform meshes. For all $\phi_m \in W_{m;\delta_m}$, the following inequalities hold:*

$$C\delta_m^{d-2} \langle \Phi_m, \Phi_m \rangle \leq \langle \mathbf{M}_\Phi \Phi_m, \Phi_m \rangle \leq C\delta_m^{d-2} \langle \Phi_m, \Phi_m \rangle ,$$

*where $\Phi_m$ is the vector of the nodal degrees of freedom of $\phi_m$ in $W_{m;\delta_m}$, and $\langle \mathbf{M}_\Phi \Phi_m, \Phi_m \rangle = \|\phi_m\|^2_{\delta,\frac{1}{2},m}$. Moreover, for all $\lambda_m \in M_{m;\delta_m}$, we have also:*

$$C\delta_m^{d} \langle \Lambda_m, \Lambda_m \rangle \leq \langle \mathbf{M}_\Lambda \Lambda_m, \Lambda_m \rangle \leq C\delta_m^{d} \langle \Lambda_m, \Lambda_m \rangle ,$$

*where $\Lambda_m$ is the vector of the degrees of freedom of $\lambda_m$ in $M_{m;\delta_m}$, and $\langle \mathbf{M}_\Lambda \Lambda_m, \Lambda_m \rangle = \|\lambda_m\|^2_{\delta,-\frac{1}{2}}$.*

The proof of this lemma can be found in [EG02] for the $L^2$ norm and the adaptation to the weighted $L^2$ norms is straightforward. As an illustration, we check numerically the satisfaction of the inf-sup condition (8) with piecewise constant $\lambda_h \in M_\delta$ and piecewise linear $\phi_h \in W^0_\delta$ with bubble stabilization. It is done on the same square interface $\mathcal{S}$ used in the previous subsection (counter example). On figure 4, we present the quantity $\frac{1}{\delta^2}\lambda_{min}(\mathbf{B}\mathbf{B}^t)^{1/2}$ as a function of $\delta$. In particular, it remains greater than a positive constant as $\delta$ goes to 0, proving (8).

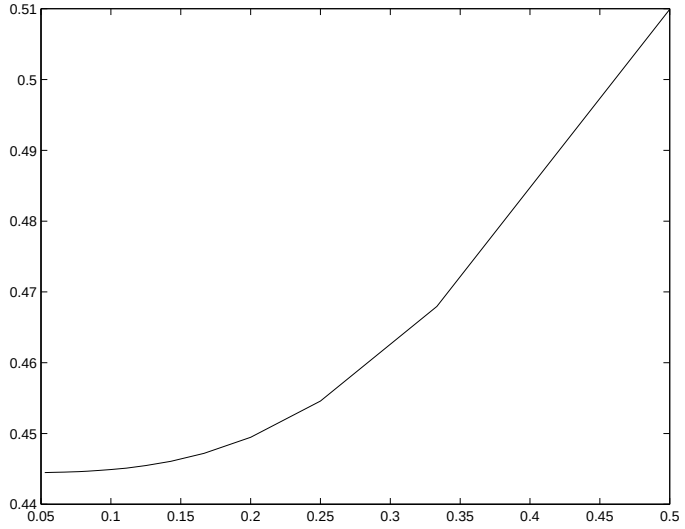


Figure 4: Numerical computation of $\frac{1}{\delta^2}\lambda_{min}(\mathbf{B}\mathbf{B}^t)^{1/2}$ as a function of $\delta$ when $\delta \to 0$.

### 3.4 A useful lemma

It can be useful to check only a local inf-sup condition on macro-elements, in the way of Boland-Nicolaides [BN83] or Stenberg [Ste84, Ste90] for divergence free problems. We assume that the interface $\mathcal{S}$ is equipped with a family of macro-meshes $(\mathcal{N}_\delta)_{\delta>0}$ constituted of macro-elements. Each macro-element $\omega \in \mathcal{N}_\delta$ is a subset $\omega \subset \mathcal{F}_\delta$ of adjacent elements.

*We assume that each element $F \in \mathcal{F}_\delta$ belong to at least one and less than $L$ macro-elements in $\mathcal{N}_\delta$, independently of $\delta$.*

Moreover, each $\omega = \cup_i F_i \in \mathcal{N}_\delta$ is assumed to be the image of a reference macroelement $\hat{\omega} = \cup_i \hat{F}_i$ by a mapping $J$, such that the restrictions $J|_{\hat{F}_i} : \hat{F}_i \to F_i$ are bounded transformations. The set of reference macro-elements is denoted by $\hat{\mathcal{N}}$.

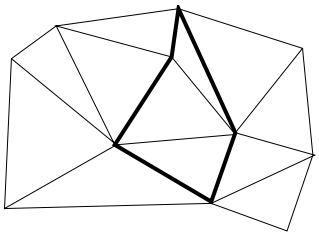

Figure 5: Example of a macro-element in a mesh.

**Lemma 2.** *Let us assume that for all reference macro-element $\hat{\omega} \in \hat{\mathcal{N}}$, we have with obvious notations:*

$$\inf_{\hat{\lambda} \in M_\delta(\hat{\omega}) \setminus \{0\}} \sup_{\hat{\phi} \in W_\delta^0(\hat{\omega}) \setminus \{0\}} \frac{\displaystyle\int_{\hat{\omega}} \hat{\phi} \cdot \hat{\lambda}}{\|\hat{\phi}\|_{L^2(\hat{\omega})} \|\hat{\lambda}\|_{L^2(\hat{\omega})}} \geq \beta_{\hat{\omega}}. \tag{10}$$

*Then (8) is satisfied for all $k \geq 1$, with a stability constant $\beta'_k \geq C \inf_{\hat{\omega} \in \hat{\mathcal{N}}} \beta_{\hat{\omega}}$.*

The proof exactly follows the arguments from Stenberg [Ste84, Ste90], and we detail it for completeness.

**Proof :** Thanks to a change of variable, the local assumptions (10) on reference macro-elements can be extended on any macro-element $\omega = J\hat{\omega}$. Indeed, for $\lambda \in M_\delta(\omega)$ and $\phi \in W_\delta^0(\omega)$:

$$\int_\omega \lambda \cdot \phi = \sum_i \int_{F_i} \lambda \cdot \phi = \sum_i \frac{meas(F_i)}{meas(\hat{F}_i)} \int_{\hat{F}_i} \hat{\lambda} \cdot \hat{u} \geq C \sum_i h(F_i)^{d-1} \int_{\hat{F}_i} \hat{\lambda} \cdot \hat{u},$$

by regularity of the mesh. Using its quasi-uniformity, we obtain:

$$\int_\omega \lambda \cdot \phi \geq C\delta^{d-1} \int_{\hat{\omega}} \hat{\lambda} \cdot \hat{\phi}.$$

We have also:

$$\begin{aligned} \|\phi\|^2_{\delta,\frac{1}{2},\omega} &= \sum_i \frac{1}{h(F_i)} \|\phi\|^2_{L^2(F_i)} \\ &= \sum_i \frac{1}{h(F_i)} \frac{meas(F_i)}{meas(\hat{F}_i)} \|\hat{\phi}\|^2_{L^2(\hat{F}_i)} \\ &\leq C\delta^{d-2} \|\hat{\phi}\|^2_{L^2(\hat{\omega})}, \end{aligned}$$

and similarly:

$$\|\lambda\|^2_{\delta,-\frac{1}{2},\omega} \leq C\delta^d \|\hat{\lambda}\|^2_{L^2(\hat{\omega})}.$$

Then, from (10), we get for all $\omega \in \mathcal{N}_\delta$:

$$\inf_{\lambda \in M_\delta(\omega) \setminus \{0\}} \sup_{\phi \in W_\delta(\omega) \cap H_0^1(\omega) \setminus \{0\}} \frac{\displaystyle\int_\omega \phi \cdot \lambda}{\|\phi\|_{\delta,\frac{1}{2},\omega} \|\lambda\|_{\delta,-\frac{1}{2},\omega}} \geq C\beta_{\hat{\omega}}. \tag{11}$$

Now, we will prove the global inf-sup condition (8). Let $\lambda \in M_\delta$. For all $\omega \in \mathcal{N}_\delta$, the condition (11) proves that there exists a function $\phi_\omega \in W^0_\delta(\omega)$ vanishing outside $\omega$ such that:

$$\int_\omega \lambda \cdot \phi_\omega \geq C\|\lambda\|^2_{\delta,-\frac{1}{2},\omega},$$

with:

$$\|\phi_\omega\|_{\delta,\frac{1}{2},\omega} \leq \|\lambda\|_{\delta,-\frac{1}{2},\omega}.$$

Let us define:

$$\phi = \sum_{\omega\in\mathcal{N}_\delta} \phi_\omega.$$

Then, because each element is in a macro-element at least and in less than $L$:

$$\int_{\mathcal{S}} \lambda \cdot \phi = \sum_{\omega\in\mathcal{N}_\delta} \int_\omega \lambda \cdot \phi_\omega \geq C \sum_{\omega\in\mathcal{N}_\delta} \|\lambda\|^2_{\delta,-\frac{1}{2},\omega}$$

$$= C \sum_{\omega\in\mathcal{N}_\delta} \sum_{F\in\omega} h(F)\|\lambda\|^2_{L^2(F)^d} = C \sum_{F\in\mathcal{F}_\delta} \sum_{\omega\ni F} h(F)\|\lambda\|^2_{L^2(F)^d}$$

$$\geq C \sum_{F\in\mathcal{F}_\delta} h(F)\|\lambda\|^2_{L^2(F)^d} = C\|\lambda\|^2_{\delta,-\frac{1}{2}},$$

and:

$$\|\phi\|^2_{\delta,\frac{1}{2}} \leq \sum_{\omega\in\mathcal{N}_\delta} \|\phi_\omega\|^2_{\delta,\frac{1}{2},\omega} \leq \sum_{\omega\in\mathcal{N}_\delta} \|\lambda\|^2_{\delta,-\frac{1}{2},\omega}$$

$$\leq \sum_{F\in\mathcal{F}_\delta} \sum_{\omega\ni F} h(F)\|\lambda\|^2_{L^2(F)^d} \leq L \sum_{F\in\mathcal{F}_\delta} h(F)\|\lambda\|^2_{L^2(F)^d} = L\|\lambda\|^2_{\delta,-\frac{1}{2}},$$

which proves (8). □

As a consequence, local inf-sup conditions has only to be checked on reference macro-elements to ensure a global inf-sup compatibility.

## 3.5 Second order stabilized interface elements

We now introduce some stabilized elements achieving second order approximation in displacements and satisfying the local inf-sup condition (10).

### 3.5.1 1D macroelements

For bidimensional problems, we build on the reference interface element $\hat{\omega} = [-1; 1]$, the following spaces:

$$\begin{cases} M_\delta(\hat{\omega}) = \mathbb{P}_1(\hat{\omega})^2, \\ W^0_\delta(\hat{\omega}) = \left(\mathbb{P}_2(\hat{\omega})^2 \oplus span\{\hat{b}\}^2\right) \cap H^1_0(\hat{\omega})^2, \end{cases}$$

where the interface bubble function $\hat{b}$ is an odd function over $[-1,1]$, which satisfies:

$$\int_0^1 x\hat{b}(x)\,dx \neq 0.$$

Then, the local inf-sup condition (10) is satisfied on a macro-element made of the single element $\hat{\omega}$. Indeed, let $\lambda \in M_\delta(\hat{\omega})$ be such that:

$$\int_{\hat{\omega}} \phi \cdot \lambda = 0, \quad \forall \phi \in W_\delta^0(\hat{\omega}).$$

For all $1 \leq i \leq 2$, denoting by $\lambda_i$ the $i$th component of $\lambda$, we have $\lambda_i(x) = \alpha_i x + \beta_i$ for $x \in \hat{\omega}$, and its integral against any second order polynomial and the bubble $\hat{b}$ vanishes, which implies:

$$\begin{cases} \displaystyle\int_{-1}^1 \lambda_i(x)(1-x^2)\,dx = \frac{4}{3}\beta_i = 0 \quad \Longrightarrow\ \beta_i = 0, \\ \displaystyle\int_{-1}^1 \lambda_i(x)\hat{b}(x)\,dx = 2\alpha_i \int_0^1 x\hat{b}(x)\,dx = 0 \quad \Longrightarrow\ \alpha_i = 0. \end{cases}$$

Therefore, $\lambda = 0$, which proves that the local inf-sup condition (10) is satisfied.

As a bubble $\hat{b}$, one can take:

$$\hat{b}(x) = x(1-x^2), \quad x \in \hat{\omega}. \tag{12}$$

Obviously, $\hat{b}$ is the trace over $\hat{\omega} \times \{0\}$ of a bubble function $\hat{h}$ defined in a reference element $\hat{K} \subset \mathbb{R}^2$, whose $\hat{\omega} \times \{0\}$ is an edge.

In the case where $\hat{K} = \hat{T}$ is a reference triangle, if $A = (-1,0)$, $B = (1,0)$ and $C = (-1,2)$ are its vertices, the interface bubble function $\hat{h}$ can be defined as:

$$\hat{h}(x,y) = \begin{cases} \left(1 - \dfrac{y}{2}\right) \hat{b}\left(\dfrac{2x+y}{2-y}\right), & \forall (x,y) \in \hat{T} \setminus (-1,2), \\ 0, \quad (x,y) = (-1,2). \end{cases}$$

Such a function $\hat{h}$ is represented on figure 6.

In the case where $\hat{K} = \hat{Q}$ is a reference square, if $A = (-1,0)$, $B = (1,0)$, $C = (1,2)$ and $D = (-1,2)$ are its corners, the interface bubble function $\hat{h}$ can be defined as:

$$\hat{h}(x,y) = \left(1 - \frac{y}{2}\right) \hat{b}\,(x)\,, \quad \forall (x,y) \in \hat{Q}.$$

Such a function $\hat{h}$ is represented on figure 7.

### 3.5.2 2D quadrangular interface macroelement

For tridimensional problems, we introduce the following second order 2D quadrilateral interface element. Let $\hat{\omega} = \hat{Q} = [-1,1]^2$ be a reference quadrilateral, on which we build the following spaces:

$$\begin{cases} M_\delta(\hat{\omega}) = \mathbb{P}_1(\hat{Q})^3, \\ W_\delta^0(\hat{\omega}) = \left(\mathbb{Q}_2(\hat{Q})^3 \oplus span\{\hat{b}_1, \hat{b}_2\}^3\right) \cap H_0^1(\hat{\omega})^3, \end{cases}$$

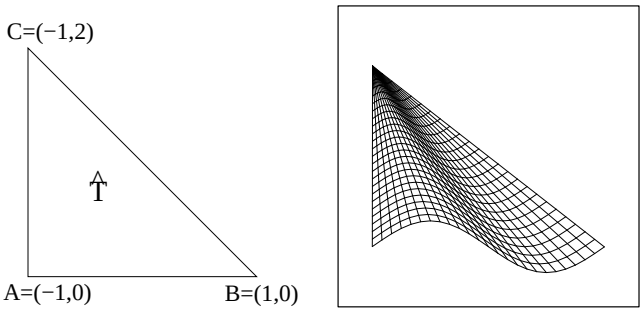


Figure 6: A reference triangle $\hat{T}$ and a corresponding interface bubble function $\hat{h}$ on the edge $[AB] = \hat{\omega} \times \{0\}$.

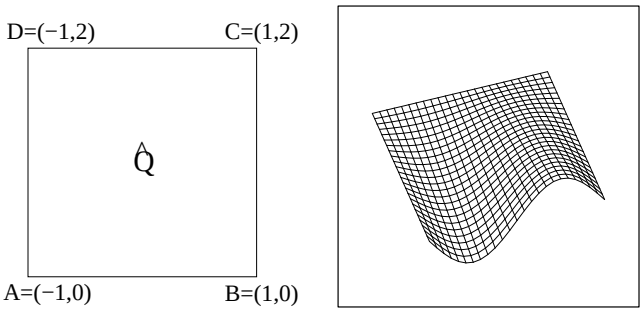


Figure 7: A reference square $\hat{Q}$ and a corresponding interface bubble function $\hat{h}$ on the edge $[AB] = \hat{\omega} \times \{0\}$.

where the bubble functions are defined as follows:

$$\hat{b}_k(x_1, x_2) = x_k(1 - x_k^2)(1 - x_l^2), \quad l \neq k, \tag{13}$$

the $(x_k)_{k=1,2}$ being the euclidian coordinates in $\mathbb{R}^2$. An illustration of such bubble functions defined on the reference square is shown on figure 8.

The corresponding element satisfies the local inf-sup condition (10) on a macro-element made of the single element $\hat{Q}$. Indeed, let $\lambda \in M_\delta(\hat{\omega})$ be such that:

$$\int_{\hat{\omega}} \phi \cdot \lambda = 0, \quad \forall \phi \in W_\delta^0(\hat{\omega}).$$

For all $1 \leq i \leq 3$, denoting by $\lambda_i$ the $i$th component of $\lambda$, we have $\lambda_i(x_1, x_2) = \alpha_i x_1 + \beta_i x_2 + \gamma_i$ for $(x_1, x_2) \in \hat{\omega}$, and its integral against any second partial order polynomial and bubble vanishes, which implies:

$$\int_{\hat{Q}} \lambda(x_1, x_2)(1 - x_1^2)(1 - x_2^2)\, dx_1\, dx_2 = \frac{16}{9}\gamma_i = 0 \quad \Longrightarrow \ \gamma_i = 0,$$

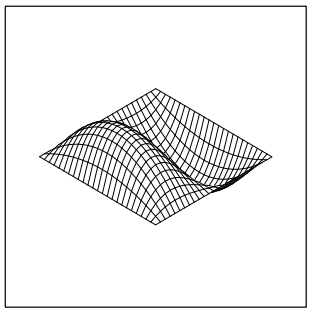

Figure 8: A bubble function defined by (13) on the reference square $\hat{Q}$.

$$\int_{\hat{Q}} \lambda(x_1,x_2)x_1(1-x_1^2)(1-x_2^2)\,dx_1\,dx_2 = \frac{16}{45}\alpha_i = 0 \quad \Longrightarrow\ \alpha_i = 0,$$
$$\int_{\hat{Q}} \lambda(x_1,x_2)x_2(1-x_1^2)(1-x_2^2)\,dx_1\,dx_2 = \frac{16}{45}\beta_i = 0 \quad \Longrightarrow\ \beta_i = 0,$$

that is $\lambda = 0$, which proves that the local inf-sup condition (10) is satisfied.

As previously, the interface bubble functions $(\hat{b}_k)_{k=1,2}$ are the restrictions to $\hat{Q}\times\{0\}$ of functions $(\hat{h}_k)_{k=1,2}$ defined on a reference cube $\hat{\mathbb{Q}} = \hat{Q}\times[0;2]$ whose $\hat{Q}\times\{0\}$ is a face. More precisely, we can define for $k = 1, 2$:

$$\hat{h}_k(x_1,x_2,x_3) = \left(1-\frac{x_3}{2}\right)\hat{b}_k(x_1,x_2), \quad \forall (x_1,x_2)\in\hat{Q}, \forall x_3\in[0,2].$$

### 3.5.3 2D triangular interface macroelement

For tridimensional problems, we introduce the following second order 2D triangular interface element. Let $\hat{\omega} = \hat{T}$ be a triangular element whose vertices are $A = (1,0)$, $B = (0,1)$ and $C = (0,0)$. We introduce the following spaces:

$$\begin{cases} M_\delta(\hat{\omega}) = \mathbb{P}_1(\hat{T})^3, \\ W^0_\delta(\hat{\omega}) = \left(\mathbb{P}_2(\hat{T})^3 \oplus span\{\hat{b}_1,\hat{b}_2,\hat{b}_3\}^3\right) \cap H^1_0(\hat{\omega})^3, \end{cases}$$

where the bubble functions are defined by:

$$\hat{b}_1 = \left(\hat{\lambda}_1 - \frac{1}{2}\right)\hat{\lambda}_1\hat{\lambda}_2\hat{\lambda}_3,$$
$$\hat{b}_2 = \left(\hat{\lambda}_2 - \frac{1}{2}\right)\hat{\lambda}_1\hat{\lambda}_2\hat{\lambda}_3,$$
$$\hat{b}_3 = \left(\hat{\lambda}_3 - \frac{1}{2}\right)\hat{\lambda}_1\hat{\lambda}_2\hat{\lambda}_3,$$

in which $\hat{\lambda}_1$, $\hat{\lambda}_2$ and $\hat{\lambda}_3$ are the barycentric coordinates on $\hat{T}$, respectively associated to the vertices $A$, $B$ and $C$. A typical example of such bubbles is given on figure 9.

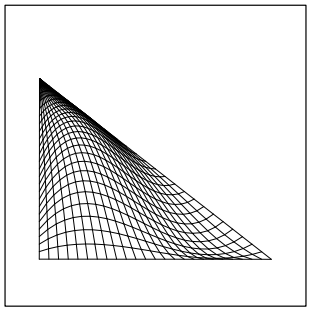

Figure 9: A bubble function on the reference interface triangle $\hat{T}$.

The corresponding element satisfies the local inf-sup condition (10) on a macro-element made of the single element $\hat{T}$. Indeed, let $\lambda \in M_\delta(\hat{\omega})$ be such that:

$$\int_{\hat{\omega}} \phi \cdot \lambda = 0, \quad \forall \phi \in W^0_\delta(\hat{\omega}).$$

For all $1 \leq i \leq 3$, denoting by $\lambda_i$ the $i$th component of $\lambda$, we have $\lambda_i = \alpha_i \hat{\lambda}_1 + \beta_i \hat{\lambda}_2 + \gamma_i \hat{\lambda}_3$, and its integral against any second partial order polynomial and bubble vanishes, which implies:

$$M \begin{pmatrix} \alpha_i \\ \beta_i \\ \gamma_i \end{pmatrix} = \begin{pmatrix} 0 \\ 0 \\ 0 \end{pmatrix}, \tag{14}$$

with:

$$M_{kl} = \int_{\hat{T}} \hat{b}_k \hat{\lambda}_l, \quad 1 \leq k, l \leq 3.$$

To compute these coefficients, we use the following lemma (see for example [Lar95], page 57):

**Lemma 3.** *Let $T$ a non-degenerated triangle in $\mathbb{R}^2$ and $\lambda_1(x)$,$\lambda_2(x)$,$\lambda_3(x)$ the barycentric coordinates of $x \in \mathbb{R}^2$ with respect to the vertices of $T$. Then:*

$$\int_T \lambda_1(x)^k \lambda_2(x)^l \lambda_3(x)^m \, dx = 2 \, meas(T) \, \frac{k! \, l! \, m!}{(k+l+m+2)!}.$$

Now, let us calculate the coefficients of the matrix $M$ by using the previous lemma. It is obtained that for $k = 1, 2, 3$:

$$\begin{aligned} M_{kk} &= \int_{\hat{T}} \left( \hat{\lambda}_1 - \frac{1}{2} \right) \hat{\lambda}_1^2 \hat{\lambda}_2 \hat{\lambda}_3 = \int_{\hat{T}} \hat{\lambda}_1^3 \hat{\lambda}_2 \hat{\lambda}_3 - \frac{1}{2} \int_{\hat{T}} \hat{\lambda}_1^2 \hat{\lambda}_2 \hat{\lambda}_3, \\ &= 2 \, meas(\hat{T}) \left( \frac{3!}{7!} - \frac{1}{2} \times \frac{2!}{6!} \right) = - \frac{2 \, meas(\hat{T})}{7!}, \end{aligned} \tag{15}$$

and that for all $k, l \in \{1,2,3\}$ such that $i \neq j$:

$$\begin{aligned} M_{kl} &= \int_{\hat{T}} \left(\hat{\lambda}_1 - \frac{1}{2}\right) \hat{\lambda}_1 \hat{\lambda}_2^2 \hat{\lambda}_3 = \int_{\hat{T}} \hat{\lambda}_1^2 \hat{\lambda}_2^2 \hat{\lambda}_3 - \frac{1}{2} \int_{\hat{T}} \hat{\lambda}_1 \hat{\lambda}_2^2 \hat{\lambda}_3 \\ &= 2\, meas(\hat{T}) \left( \frac{2!\,2!}{7!} - \frac{1}{2} \times \frac{2!}{6!} \right) = -3 \times \frac{2\, meas(\hat{T})}{7!}. \end{aligned}$$

Then:

$$-\frac{7!}{2\, meas(\hat{T})} M = \begin{pmatrix} 1 & 3 & 3 \\ 3 & 1 & 3 \\ 3 & 3 & 1 \end{pmatrix},$$

and the original linear system (14) is equivalent to:

$$\begin{pmatrix} 1 & 3 & 3 \\ 3 & 1 & 3 \\ 3 & 3 & 1 \end{pmatrix} \begin{pmatrix} \alpha_i \\ \beta_i \\ \gamma_i \end{pmatrix} = \begin{pmatrix} 0 \\ 0 \\ 0 \end{pmatrix}.$$

The right hand side matrix is invertible, and the only solution is then $\alpha_i = \beta_i = \gamma_i = 0$ for all $1 \leq i \leq 3$, that is $\lambda = 0$, which proves that the local inf-sup condition (10) is satisfied.

As previously, the interface bubble functions $(\hat{b}_k)_{k=1,2,3}$ are the restrictions to $\hat{T} \times \{0\}$ of functions $(\hat{h}_k)_{k=1,2,3}$ defined on a reference tetrahedron $\hat{\mathbb{T}}$ whose $\hat{T} \times \{0\}$ is a face. More precisely, if $\lambda_1, ..., \lambda_4$ are the barycentric coordinates associated to the vertices of $\hat{\mathbb{T}}$, and assuming that $\lambda_4$ is the barycentric coordinate associated to the node not belonging to $\hat{T} \times \{0\}$, we have for $k = 1, 2, 3$:

$$\hat{h}_k = \lambda_k (\lambda_k - \frac{1}{2}) \lambda_l \lambda_m (1 - \lambda_4), \quad \{l, m\} = \{1,2,3\} \setminus \{k\}.$$

# 4 Some numerical issues

The practical implementation of mortar elements such as those introduced in the above sections, faces a few technical problems outlined in this section.

## 4.1 Penalized formulation.

One can replace the solution of a saddle-point problem by the solution of a positive definite one, by introducing a penalized formulation for (6). It is a very standard solution in many academic and industrial implementations for treating kinematic constraints and non-homogenous essential boundary conditions. Herein, we propose a mesh-dependent penalization term. Introducing the following $L^2$ inner product:

$$c(\lambda, \mu) = \int_{\mathcal{S}} \lambda \cdot \mu, \quad \forall \lambda, \mu \in M_\delta,$$

and denoting by $\eta > 0$ a small penetration parameter, we propose to replace the problem (6) by the symmetric positive definite one:

$$\begin{cases} \tilde{a}(u_h^\eta, v_h) + b(v_h, \lambda_h^\eta) = l(v_h), & \forall v_h \in X_h, \\ b(u_h^\eta, \mu_h) = \eta\, \delta_{min}\, c(\lambda_h^\eta, \mu_h), & \forall \mu_h \in M_\delta, \end{cases} \tag{16}$$

where the minimum diameter of interface surfacic elements has been denoted by:

$$\delta_{min} = \min_{F \in \mathcal{F}_\delta} h(F).$$

Then, one can prove (following [EG02] for example) the convergence of the penalized solution of the system (16) to the exact constrained solution of (6) as $\eta$ goes to zero:

**Proposition 3.** *We assume that the original mortar formulation (6) is well-posed in the sense of Part I, with quasi-uniform meshes on the interfaces, and denote by $(u_h, \lambda_h) \in X_h \times M_\delta$ its unique solution. Then, for all $\eta > 0$, there exists a unique solution $(u_h^\eta, \lambda_h^\eta) \in X_h \times M_\delta$ of (16), and the convergence of the penalized solution to $(u_h, \lambda_h)$ as $\eta \to 0$ holds in the sense that:*

$$\|u_h - u_h^\eta\|_X \leq C\ \eta,$$

$$\|\lambda_h - \lambda_h^\eta\|_{\delta,-\frac{1}{2}} \leq C\ \eta,$$

*where $C$ denotes various constants independent of the penalization coefficient $\eta$, of the decomposition into subdomains, and the discretization.*

The penalized formulation reinforces the interest in mesh-dependent formulations. We insist on the presence in the penalty term of the minimum diameter of the surfacic interface elements $\delta_{min}$, which is of crucial importance to obtain constants independent of the discretization in convergence estimates with respect to the penalization coefficient $\eta$, because we have $\delta_{min} c(\lambda, \lambda) \simeq \|\lambda\|^2_{\delta,-\frac{1}{2}}$. In spite of the practical computational interest of such a penalized formulation, it is recalled that the condition number classically explodes like $O(1/\eta)$, which suggests that a good compromise should be chosen on the value of the penalization coefficient $\eta$.

## 4.2 Exact integration of the constraint

From the numerical point of view, especially in 3D, the accurate calculation of the integral $\int_\Gamma \phi_h \cdot \lambda_h$ is difficult when $\phi_h$ and $\lambda_h$ do not live on the same side of the interface $\Gamma$, and are therefore defined on completely independent meshes.

The question of approximating this integral by quadrature has been risen in [CLM97, MRW02]. The authors prove that any approximation of this integral by quadrature either on the mortar or non-mortar side is not optimal, leading to a convergence in "$\sqrt{h}$". This bad behavior will be illustrated in the numerical results to follow. A dissymetric formulation in which this integral is always approximated by quadrature is proposed.

Herein, we have decided to compute exactly such an integral because the simplest quadrature approach does not lead to accurate simulations as illustrated on figure 13 of the next section, and have giving it up using the non-symmetric approach from [CLM97, MRW02].

More precisely, let $\phi_h$ a finite element displacement living on the mortar side of the interface, and $P$ an interface element on the same side, where $\phi_h$ does not vanish. Let $Q$ an interface element of the non-mortar side having a non-empty intersection with $P$, and where the finite element Lagrange multiplier $\lambda_h$ does not vanish. To compute the integral $\int_{P \cap Q} \phi_h \cdot \lambda_h$, we proceed as follows:

1. We compute the exact intersection of the convex polygons $P$ and $Q$ (see figure 10), for which we refer to the book of Joseph O'Rourke [O'R82] for example. The code source in C can be downloaded on his website. It is originally written in integer precision, but can be modified to deal with double precision, and also to detect the complete inclusion of a polygonal into another.
2. We introduce the barycentre $G$ of the $n$ vertices of the intersection polygon $P \cap Q$, and decompose it into $n$ triangles sharing the same vertex $G$ as illustrated on figure 10. We denote $P \cap Q = \cup_{i=1}^{n} T_i$.
3. For all $i = 1, .., n$, the integral $\int_{T_i} \phi_h \cdot \lambda_h$ is computed exactly by quadrature, since $\phi_h \cdot \lambda_h$ is a polynomial over $T_i$. The exact integration is then obtained by:

$$\int_{P \cap Q} \phi_h \cdot \lambda_h = \sum_{i=1}^{n} \int_{T_i} \phi_h \cdot \lambda_h,$$

the last term being computed thanks to lemma 3.

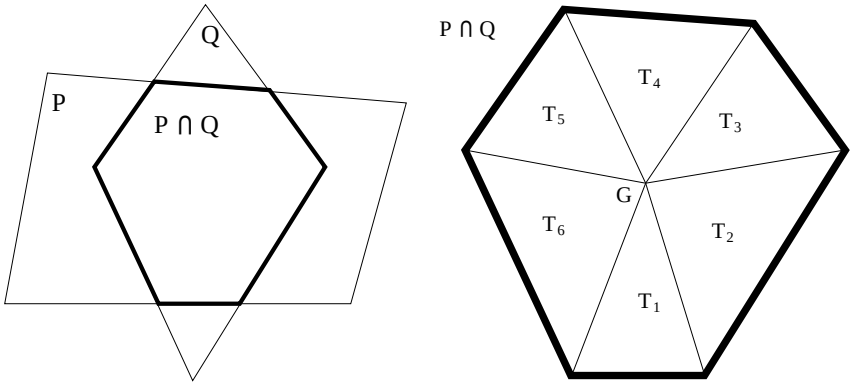


Figure 10: The exact intersection of the convex polygons $P$ and $Q$, and its decomposition into triangles.

**Remark 4.** *A major practical problem concerns the case when the discretization of the mortar and non-mortar interfaces do not geometrically match. Sometimes, in the case of second order approximation for the displacements, an isoparametric discretization of the interface enables perfect geometric matching and the work done by [FMW04] ensures optimal properties. Nevertheless, in real life cases, such a matching often proves to be impossible and the reformulation of the interface weak-continuity constraint on a regularized interface is crucial, especially when dealing with non-linear elasticity. Indeed, stress singularity on the non-mortar interface may occur during large deformations if this interface is not regularized, and Newton's method convergence is then compromised. Some interesting works regarding these aspects have been published by T. Laursen and M. Puso, and propose Gregory or Hermite patch regularization of the interface (see [PL02, PL03, Pus04]). Such contributions deal also with the treatment of contact surfaces.*

# 5 Numerical tests for discontinuous mortar-elements

First, we consider an homogeneous beam made with a Hooke's material, whose a tip is clamped on a wall, and whose the other tip is under traction by a uniform negative pressure. All the characteristics are detailed in the table, figure 11. For comparison purpose, both non-conforming and conforming meshes are considered, as shown on figure 12. They are respectively made of 2926 nodes with 2240 elements and 4225 nodes with 3456 elements.

| | |
|---|---|
| Young modulus $E$ | 5000 Pa |
| Poisson coefficient $\nu$ | 0.2 |
| density $\rho$ | 1 kg/m3 |
| traction pressure $p$ | 10000 Pa |
| length $L$ | 2 m |
| thickness $l$ | 1 m |
| extension under static loading | 3.97 m |
| period of the first extensional eigenmode | 0.1125 s |

Figure 11: Characteristics of the beam and first numerical estimations.

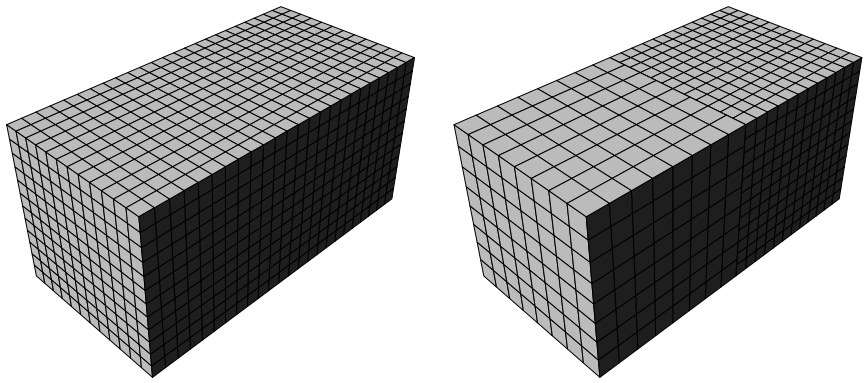

Figure 12: Conforming (4225 nodes, 3456 elements) and non-conforming (2926 nodes, 2240 elements) meshes of a beam using first order elements.

We test the proposed first order formulation by using a $\mathbb{Q}_1$ approximation for the displacements on both conforming and non-conforming models, enriched with an interface bubble stabilization (defined on the finer side of the interface) for the non-conforming model together with $\mathbb{P}_0$ Lagrange multipliers on the finer side of the interface (non-mortar side) as described in section 3.1 (page 8). We start by illustrating the non-optimal results obtained when computing the mortar constraint by quadrature on the finer side of the interface. The quadrature is exact for computing $\int_\Gamma \mu_h \cdot v_h$ when both

$\mu_h$ and $v_h$ live on the finer side of the interface. Such a computation leads to interface oscillations of the displacements, as shown on figure 13. This result confirms the work of [CLM97, MRW02], and we will definitively use the exact integration technique described in section 4.2.

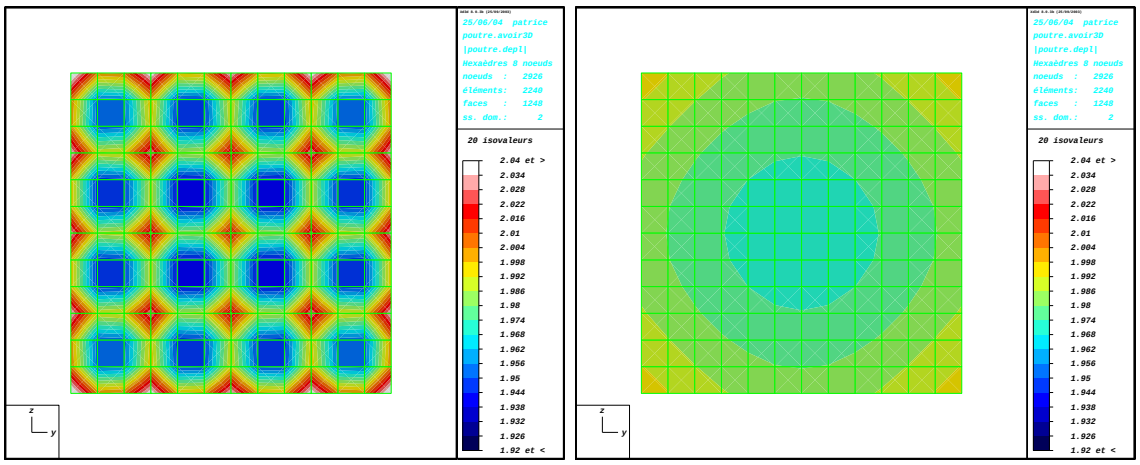


Figure 13: Interface displacements on the finer side, when using a quadrature approximation (left) and the exact integration (right) of the mortar constraint.

First, we observe the $L^\infty(\Omega)^d$-norm of the error between the displacements obtained on the conforming model and the non-conforming model on which a penalized formulation of the mortar constraint is adopted, that is $\|u_{h,conforming} - u^\eta_{h,non-conforming}\|_{L^\infty(\Omega)^d}$, as a function of the penalization coefficient $1/\eta$. The convergence process is illustrated on figure 14. By the triangular inequality, we have:

$$\|u_{h,conforming} - u^\eta_{h,non-conforming}\|_{L^\infty(\Omega)^d} \leq$$

$$\leq \|u_{h,conforming} - u_{h,non-conforming}\|_{L^\infty(\Omega)^d} + \|u_{h,non-conforming} - u^\eta_{h,non-conforming}\|_{L^\infty(\Omega)^d}.$$

For $1/\eta \leq 10^{10}$, the first term appears to be negligible, and the linear convergence is observed. At the penalization limit, the error in displacements between the conforming and non-conforming models is about $5.10^{-6}m$ in $L^\infty$ norm. The corresponding relative error is about $10^{-6}$. Concerning Cauchy stresses, a $4.10^{-4}$ relative gap between the conforming and non-conforming models is observed. This very good agreement is illustrated on figure 15, where the computed distribution of $\sigma_{11}$ stresses is represented. Finally, let us discuss the influence of the choice of the non-mortar side (defining the multipliers either on the coarse side, or on the fine one) on the solution. The relative gap of the displacements (resp. of the $\sigma_{11}$ stresses) in $L^\infty$ norm between the non-conforming solutions computed with these choices is $2.10^{-6}$ (resp. $8.10^{-4}$). As illustrated on figure 17, the relative gap of stresses remains concentrated on the elements sharing the interface. The relative gaps in displacements and stresses have the same order than the relative gaps between the conforming and non-conforming solutions. Therefore, the static analysis is confirmed (at least in a homogeneous model),

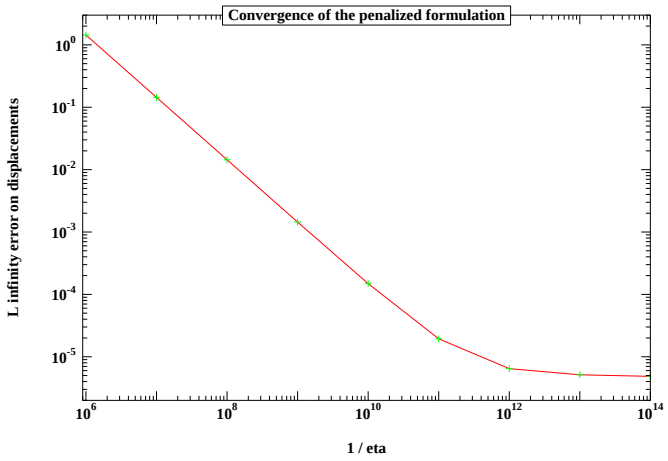


Figure 14: Error in displacements $\|u_{h,conforming} - u^{\eta}_{h,non-conforming}\|_{L^\infty(\Omega)^d}$ as a function of the penalization coefficient $1/\eta$, with $\|u_{h,conforming}\|\|_{L^\infty(\Omega)^d}$= 3.97 m .

indicating that the choice of the non-mortar side can be done on both sides without affecting the convergence.

The same simulations have been computed for a $\mathbb{Q}_2$ approximation of the displacements both on conforming and non-conforming models, using the interface stabilization presented in section 3.5, and $\mathbb{P}_1$ Lagrange multipliers. For this second order approximation, we have kept the same number of nodes than the previous first order approximation. Then, the conforming model is made with 4225 nodes and 432 elements, and the non-conforming one with 2926 nodes and 280 elements. We have adopted the value $1/\eta = 10^{11}$ of the penalization coefficient. Then, the relative gap of displacements (resp. maximal stresses) in $L^\infty$ norm between conforming and non-conforming models is $3.10^{-6}$ (resp. $1.10^{-3}$). The distribution of $\sigma_{11}$ stresses for the conforming and non-conforming models is represented on figure 16. Moreover, we show on figure 17 that the influence of the choice of the non-mortar side (defining the multipliers either on the coarse side, or on the fine one) is again rather small in this case. Indeed, the relative gap of the $\sigma_{11}$ stresses between the solutions for the two possible choices of the non-mortar side is always smaller than $2.10^{-3}$, keeping the same order than the gap in stresses between the conforming and non-conforming solutions. It is worth noticing that whereas the relative gap of displacements between the first and second order models is $2.10^{-4}$ in $L^\infty$ norm, the maximal stress has been increased by 10% in the second order model, due to the presence of a singularity at the corners of the fixed tip of the beam.
Let us now consider the elastodynamics problem associated with the previous beam model, by using the trapezoidal time discretization given by (7). For comparison purpose, the first order conforming and non-conforming space discretizations used above in the static case are tested. Here, the non-mortar side is the finer one. A

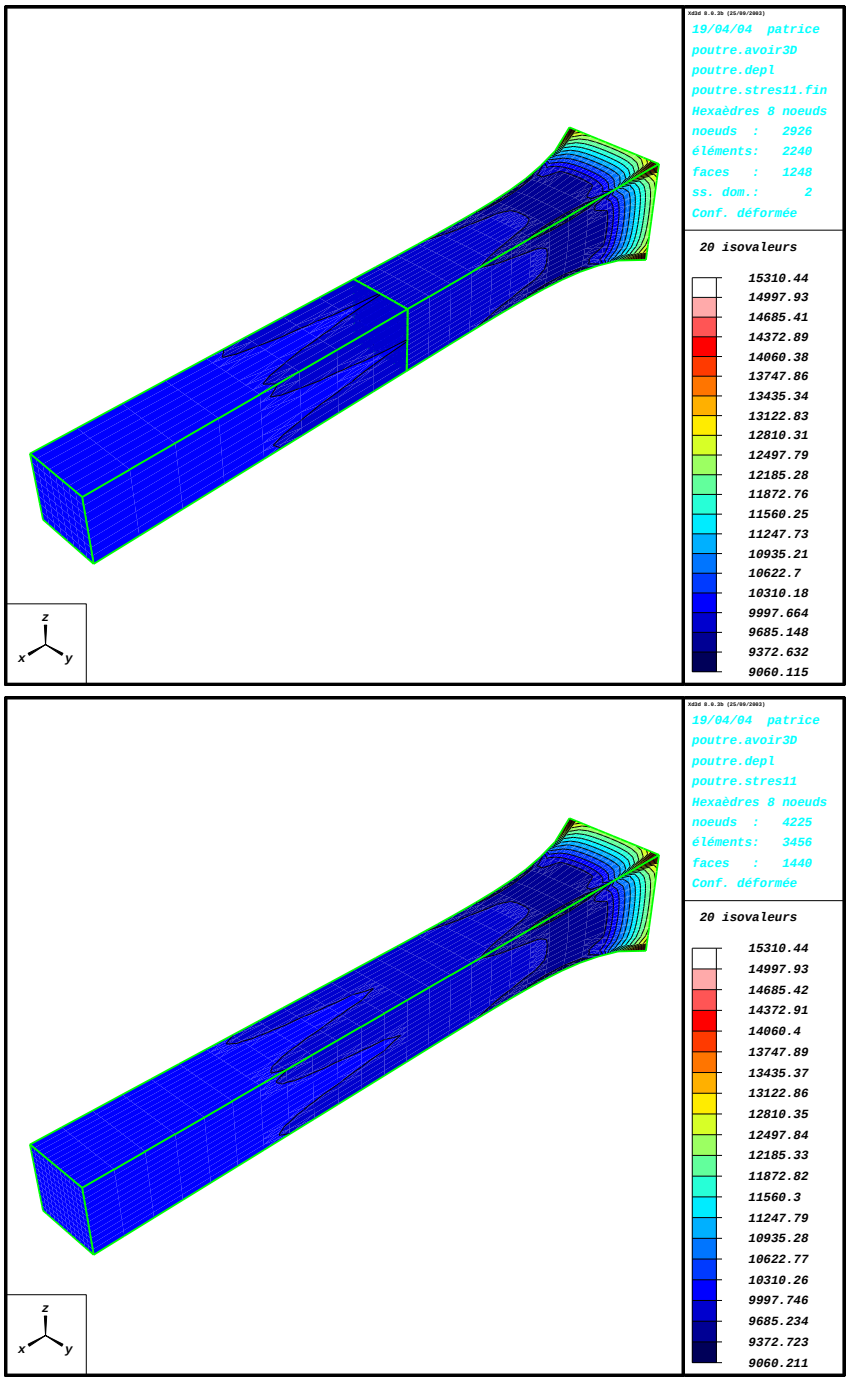


Figure 15: Distribution of $\sigma_{11}$ stresses on the deformed configuration of the non-conforming (top) and conforming (bottom) models, by using a first order approximation for the displacements.

constant traction (identical to the static case) is applied at the tip of the beam. As this sollicitation is derived from a potential, oscillations are expected and observed. Some snapshots of the computed dynamics are given on figure 18. In order to compare the space non-conforming solution with the conforming one, the horizontal displacement of the central node of the free tip of the beam is represented on figure 19 both for non-conforming and conforming approximations when using 20, 50 and 100 time steps per oscillation period. The proximity of the solutions confirms the theoretical result of optimality of the space non-conforming approximation in linear elastodynamics.
Finally, an homogeneous bidimensional cylinder in plane displacements under pressure is considered. It is made with a Hooke's material and its characteristics are given on table, figure 21. As previously, for comparison purpose, we consider both conforming and non-conforming meshes, respectively constituted of 1456 nodes with 1350 elements and 973 nodes with 810 elements, shown on figure 20. The displacements are approximated by $\mathbb{Q}_1$ polynomials, together with a bubble interface stabilization and $\mathbb{P}_0$ Lagrange multipliers, as presented in section 3.1 (page 8). In that case, the non-mortar and mortar interfaces do not geometrically match. Then, to formulate the weak-continuity constraint, the displacements of the mortar side are projected on the non-mortar side by elementary plane projections on the non-mortar faces. Of course, the previous analysis do not take this approximation into account. A better approach would have been to consider a $\mathbb{Q}_2$ approximation for the displacements, with an isoparametric description of the interface as recently analyzed in [FMW04]. Nevertheless, the bold approach presented proves to provide good results in that simple case. The distribution of maximal stresses over the deformed configuration is represented on figure 22, both for conforming and non-conforming first order approximations. The quality of the non-conforming approximation shows here the small influence of the geometric non-conformity. The influence of the choice of the non-mortar side is also studied, and the relative gap of the maximal stresses between the two possible choices is represented on figure 23. Because of the homogeneity of the material and because the non-conforming interface is not in a high stress region, such an influence remains very small.

From a practical point of view in the case of discontinuous mortar elements, let us underline that when dealing with a penalized formulation of the mortar constraint, or the elimination of the constraint as well, the assembling of the stiffness matrix of the problem in displacements can be done in a purely local way due to the discontinuity of the Lagrange multipliers. Indeed, in the corresponding stiffness operator:

$$\tilde{\mathcal{A}} + \frac{1}{\eta\,\delta_{min}}\mathcal{B}^t\mathcal{C}^{-1}\mathcal{B} = \tilde{\mathcal{A}} + \frac{1}{\eta\,\delta_{min}}\sum_{F\in\mathcal{F}_\delta}\mathcal{B}_F^t\mathcal{C}_F^{-1}\mathcal{B}_F,$$

with the natural operator notation coming from (16), the second term can be computed element by element. Moreover, no special treatment is needed on the boundary of the interfaces, which is a great advantage in terms of implementation. The price to pay for these numerical advantages lies in the implementation of the proposed bubble stabilization.

# 6 Conclusion

In this two-part paper, we have extended the classical mortar analysis to the elastodynamics framework, have shown that the mortar method is not affected by the number, the size and the shape of the subdomains (chosen sufficiently regular) both in the static and dynamic cases, and have proposed a discontinuous stabilized formulation in which the kinematic constraint is more local than usual. Tests have also been performed to confirm the theoretical work.

Beyond the analysis proposed by our contribution, an extension to the geometrically non-conforming framework appears to be necessary from the practical point of view, and the interested reader can look at the early analysis proposed in [FMW04] or at the formulation with patch introduced in [PL02, PL03, Pus04].

# References


[AT95] A. Agouzal and J.M. Thomas. Une méthode d'éléments finis hybrides en décomposition de domaines. *RAIRO M2AN*, 29:749–764, 1995.

[BCI00] K.J. Bathe, D. Chapelle, and A. Iosilevich. An inf-sup test for shell finite elements. *Computers and Structures*, 75(5):439–456, 2000.

[BD98] D. Braess and W. Dahmen. Stability estimates of the mortar finite element method for 3-dimensional problems. *East-West J. Numer. Math.*, 6:249–263, 1998.

[Bel99] F. Ben Belgacem. The mortar finite element method with lagrange multipliers. *Numer. Math.*, 84:173–197, 1999.

[BM97] F. Ben Belgacem and Y. Maday. The mortar element method for three dimensional finite element. *M2AN*, 31:289–303, 1997.

[BM00] F. Brezzi and D. Marini. Error estimates for the three-field formulation with bubble stabilization. *Math. Comp.*, 70:911–934, 2000.

[BMP93] C. Bernardi, Y. Maday, and A.T. Patera. *Asymptotic and numerical methods for partial differential equations with critical parameters*, chapter Domain decomposition by the mortar element method., pages 269–286. 1993.

[BMP94] C. Bernardi, Y. Maday, and A.T. Patera. *Nonlinear partial differential equations and their applications.*, chapter A new nonconforming approach to domain decomposition: the mortar element method., pages 13–51. Pitman, Paris, 1994.

[BN83] J. Boland and R. Nicolaides. Stability of finite elements under divergence constraint. *SIAM Numer. Anal.*, 20(4):722–731, 1983.

[CLM97] L. Cazabeau, C. Lacour, and Y. Maday. Numerical quadratures and mortar methods. In John Wiley and Sons, editors, *Computational Science for the 21st Century*, pages 119–128, 1997.

[DL72] G. Duvaut and J-L. Lions. *Les inéquations en Mécanique et en Physique.* Dunod, 1972.

[EG02] A. Ern and J-L. Guermond. *Eléments finis: théorie, applications, mise en oeuvre*, volume 36 of *collection Mathématiques et Applications*. Springer-Verlag, 2002. Also available in english as the reference [EG04].

[EG04] A. Ern and J.-L. Guermond. *Theory and Practice of Finite Elements*, volume 159 of *Applied Mathematical Series*. Springer-Verlag, New York, 2004.

[FMW04] B. Flemisch, J.M. Melenk, and B. Wohlmuth. Mortar methods with curved interfaces. Technical report, Max Planck Institute, 2004. Preprint.

[GR86] V. Girault and P-A. Raviart. *Finite element methods for Navier-Stokes equations: theory and algorithms*. 1986.

[Lar95] B. Larrouturou. *Méthodes numériques pour les sciences de l'ingénieur*. Cours de l'Ecole Polytechnique, 1995.

[MRW02] Y. Maday, F. Rapetti, and B. Wohlmuth. The influence of quadrature formulas in 3d mortar methods. In *Recent Developments in Domain Decomposition Methods, Lecture Notes in Computational Science and Engineering*, volume 23, pages 203–221. Springer, 2002.

[O'R82] J. O'Rourke. A new linear algorithm for intersecting convex polygons. *Comput. Graph Image Processing*, 19:384–391, 1982.

[PL02] M.A. Puso and T.A. Laursen. A 3d contact smoothing method using gregory patches. *International Journal for Numerical Methods in Engineering*, 54:1161–1194, 2002.

[PL03] M.A. Puso and T.A Laursen. Mesh tying on curved surfaces in 3d. *Engineering Computations*, 20:305–139, 2003.

[Pus04] M.A. Puso. A 3d mortar method for solid mechanics. *Int. J. Num. Meth. Engr.*, 59:315–336, 2004.

[Ses98] P. Seshaiyer. *Non-conforming hp finite element methods*. PhD thesis, University of Maryland, 1998.

[Ste84] R. Stenberg. Analysis of mixed finite element methods for the stokes problem: a unified approach. *Math. of Comp.*, 42:9–23, 1984.

[Ste90] R. Stenberg. A technique for analysing finite element methods for viscous incompressible flow. *Int. J. Num. Meth. Fluids*, 11:935–948, 1990.

[Woh99] B.I. Wohlmuth. Hierarchical a posteriori error estimators for mortar finite element methods with lagrange multipliers. *SIAM J. Numer. Anal.*, 36:1636–1658, 1999.

[Woh00] B.I. Wohlmuth. A mortar finite element method using dual spaces for the lagrange multiplier. *SIAM J. Numer. Anal.*, 38:989–1012, 2000.

[Woh01] B.I. Wohlmuth. *Discretization methods and iterative solvers based on domain decomposition*. Springer, 2001.

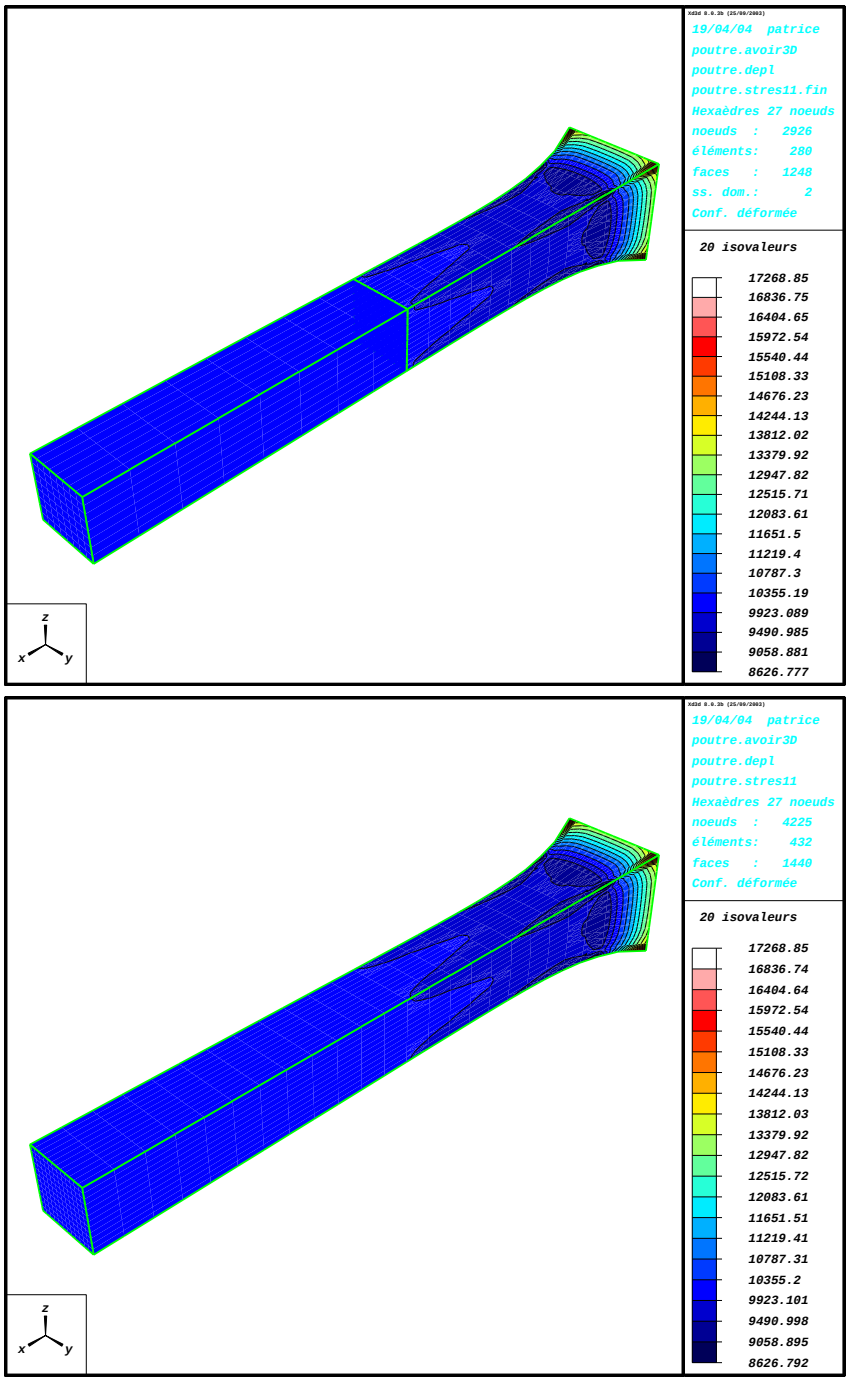


Figure 16: Distribution of $\sigma_{11}$ stresses on the deformed configuration of the non-conforming (top) and conforming (bottom) models, by using a second order approximation for the displacements.

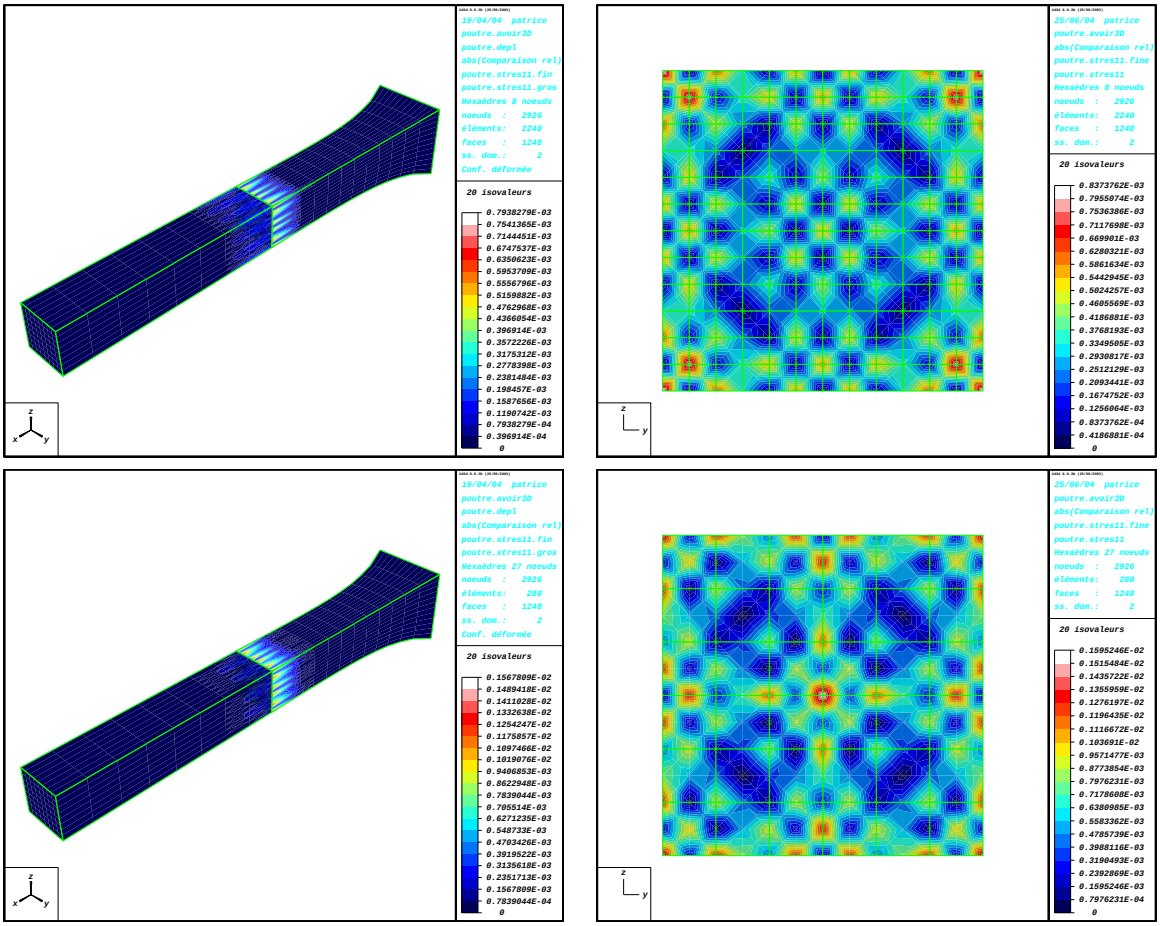


Figure 17: Relative gap of $\sigma_{11}$ stresses between the solutions computed on the non-conforming model for the two possible choices of the non-mortar side, when using a first order (top) and a second order (bottom) approximation for the displacements. The pictures on the right column are zooms on the finer side of the interface.

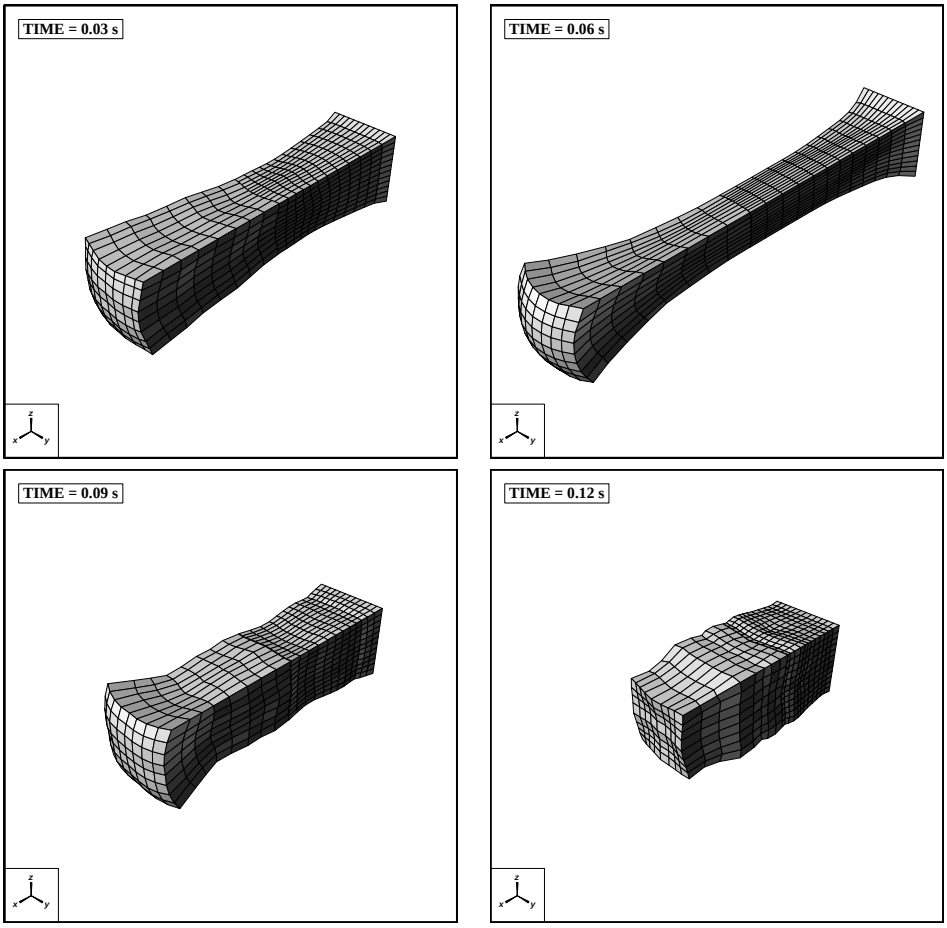


Figure 18: Snapshots of the computed dynamics of the beam by using a non-conforming first order approximation of the displacements.

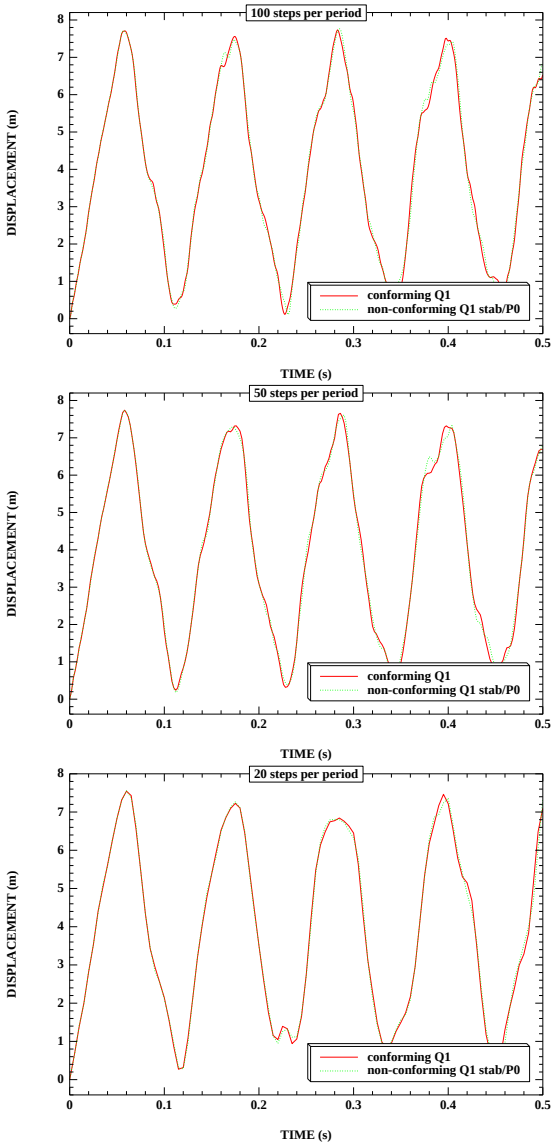


Figure 19: Horizontal displacement of the central node of the tip of the beam as a function of time, both for the non-conforming and conforming first order space approximation of the beam, together with a trapezoidal approximation in time. Simulations done with 20, 50 and 100 time steps per period. The good agreement confirms the optimality of the non-conforming space approximation.

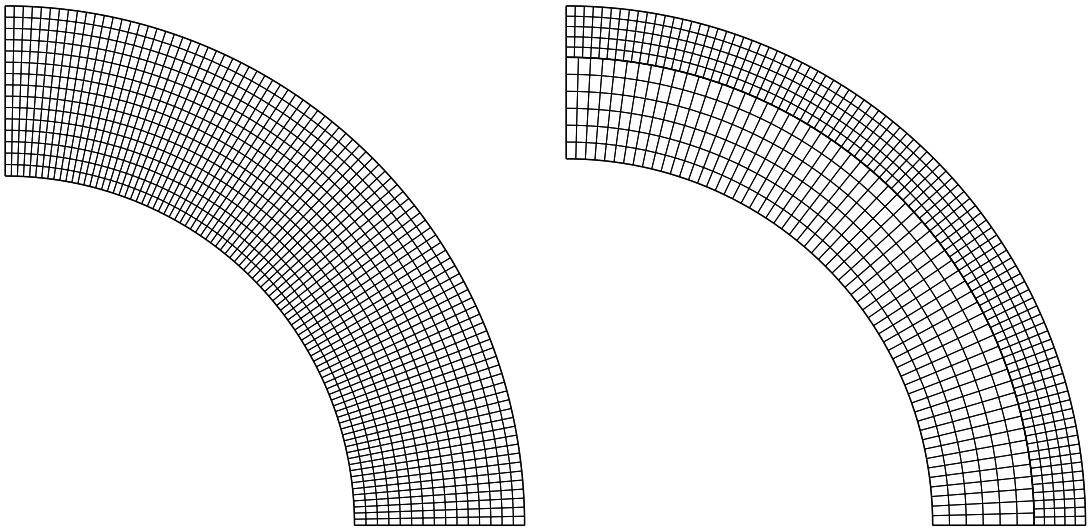

Figure 20: Conforming (1456 nodes, 1350 elements) and non-conforming (973 nodes, 810 elements) meshes of a cylinder in plane displacements.

| | |
|---|---|
| Young modulus $E$ | 5000 Pa |
| Poisson coefficient $\nu$ | 0.2 |
| internal pressure $p$ | 100 Pa |
| internal radius | 1.0 m |
| interface radius | 1.33 m |
| external radius | 1.5 m |
| maximal displacement under loading | 0.058 m |

Figure 21: Characteristics of the cylinder.

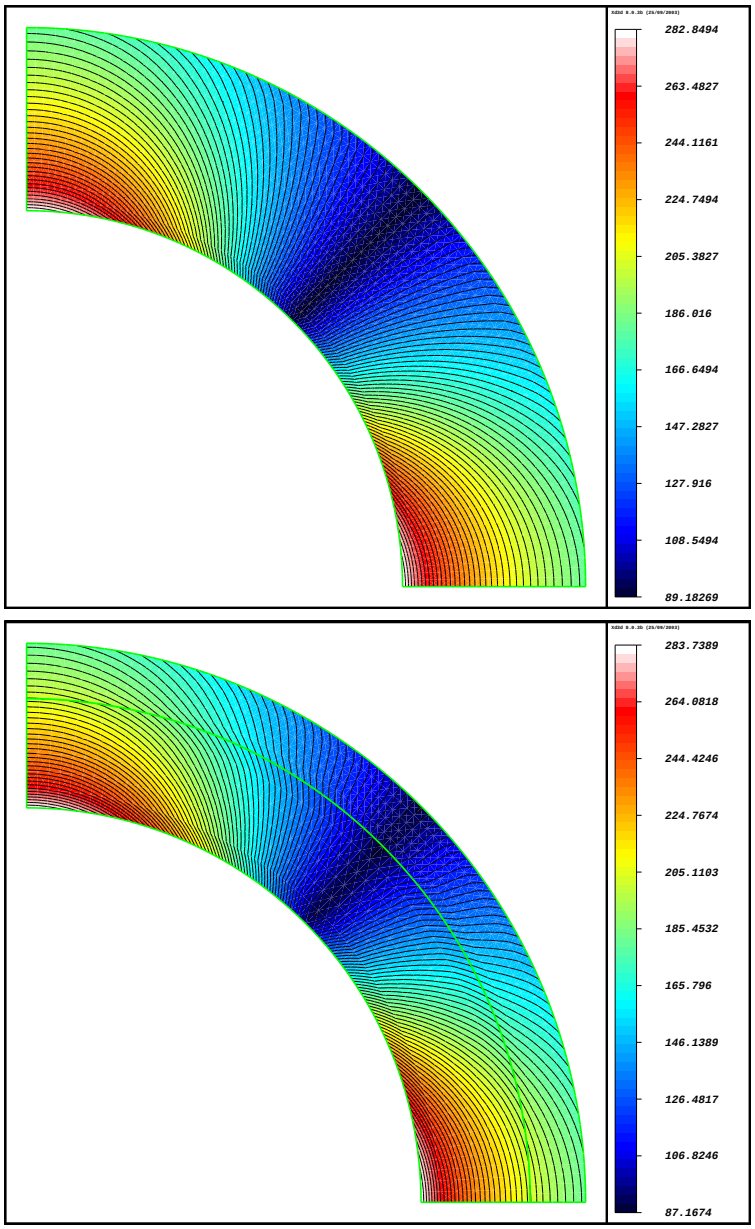


Figure 22: Distribution of the maximal stresses in a cylinder under pressure both for conforming and non-conforming space approximation.

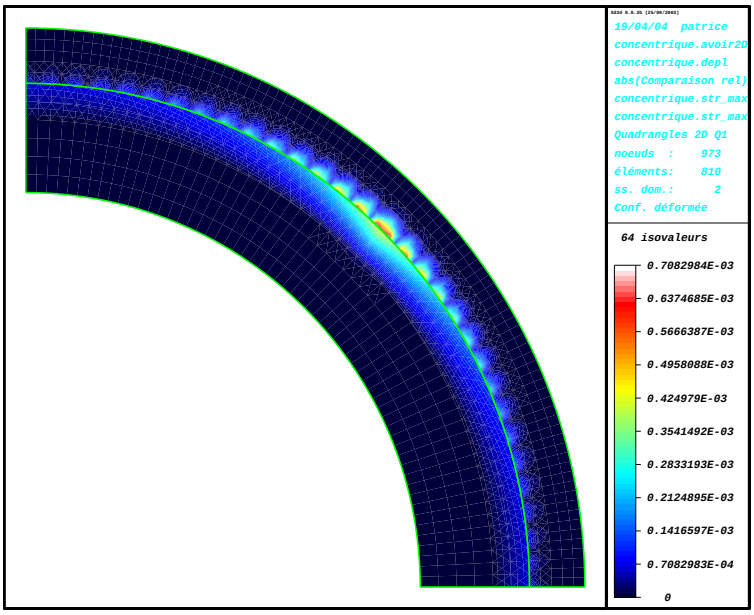


Figure 23: Relative gap of the $\sigma_{11}$ stresses between the solutions computed on the non-conforming model for the two possible choices of the non-mortar side, when using a stabilized first order approximation for the displacements and piecewise constant Lagrange multipliers.